Review article

Sasan Fathpour*

Emerging heterogeneous integrated photonic platforms on silicon

Abstract: Silicon photonics has been established as a mature and promising technology for optoelectronic integrated circuits, mostly based on the silicon-on-insulator (SOI) waveguide platform. However, not all optical functionalities can be satisfactorily achieved merely based on silicon, in general, and on the SOI platform, in particular. Long-known shortcomings of silicon-based integrated photonics are optical absorption (in the telecommunication wavelengths) and feasibility of electrically-injected lasers (at least at room temperature). More recently, high two-photon and free-carrier absorptions required at high optical intensities for third-order optical nonlinear effects, inherent lack of second-order optical nonlinearity, low extinction ratio of modulators based on the free-carrier plasma effect, and the loss of the buried oxide layer of the SOI waveguides at mid-infrared wavelengths have been recognized as other shortcomings. Accordingly, several novel waveguide platforms have been developing to address these shortcomings of the SOI platform. Most of these emerging platforms are based on heterogeneous integration of other material systems on silicon substrates, and in some cases silicon is integrated on other substrates. Germanium and its binary alloys with silicon, III–V compound semiconductors, silicon nitride, tantalum pentoxide and other high-index dielectric or glass materials, as well as lithium niobate are some of the materials heterogeneously integrated on silicon substrates. The materials are typically integrated by a variety of epitaxial growth, bonding, ion implantation and slicing, etch back, spin-on-glass or other techniques. These wide range of efforts are reviewed here holistically to stress that there is no pure silicon or even group IV photonics *per se*. Rather, the future of the field of integrated photonics appears to be one of heterogenization, where a variety of different materials and waveguide platforms will be used for different purposes with the common feature of integrating them on a single substrate, most notably silicon.

Keywords: integrated photonics; integrated optics; silicon photonics; mid-infrared photonics; optoelectronics; electrooptics; photodetectors; semiconductor lasers; optical modulators; nonlinear optics; silicon; germanium; gallium arsenide; indium phosphide; tantalum pentoxide; silicon nitride; silicon dioxide; lithium niobate.

DOI 10.1515/nanoph-2014-0024
Received September 20, 2014; accepted December 16, 2014

1 Introduction

The word "photonics" was coined over thirty 30 ago in analogy to "electronics". Since then, several related terms, such as microphotonics, integrated photonics and optoelectronic integrated circuits (OEICs), have been adopted and commonly used in analogy to microelectronics, integrated electronics, etc. Several similarities between the two fields – including using more or less the same family of materials (most notably semiconductors), the possibility of integrating several micrometer- to submicrometer-size devices on a single chip, fabrication methods based on well-established techniques conducted in cleanroom facilities – were and still are implicit in this analogy. However, as discussed below, the microelectronic chips have been increasingly dominated by the complementary metal-oxide-semiconductor (CMOS) technology, while a ubiquitous platform for microphotonics has been elusive. Instead, different photonic materials and technologies have been developed for different purposes and if there has been any path to integration, it has been one of heterogeneously merging these different platforms. This article reviews how the field of integrated photonics has been drifting into such heterogeneous integrated solutions, especially on silicon substrates.

***Corresponding author: Sasan Fathpour,** CREOL, The College of Optics and Photonics and Department of Electrical Engineering and Computer Science, University of Central Florida, 4304 Scorpius St., Orlando, FL 32816-2700, USA, e-mail: fathpour@creol.ucf.edu

Edited by Volker Sorger

In layman's terms, the story of microelectronic platforms, to a large extent, has been one of unification, while that of microphotonics has been one of balkanization. It is true that heterogeneous technologies, such as BiCMOS – a hybrid platform based on silicon-germanium (SiGe) heterojunction bipolar transistors (HBTs) and CMOS field-effect transistors – as well as III–V compound-semiconductor-based HBTs and high-electron-mobility-transistors (HEMTs) have their own important applications and market share, but the microelectronics industry, particularly at very-large scale of integration, has been dominated by Si CMOS. The reasons for this converging force of CMOS are perhaps beyond the scope of this work but briefly include the electronic design advantages of the architecture in terms of high input impedance, negligible static power consumption, self-isolation, as well as ease of layout, very high yield and scalability of the process, relative inexpensiveness of high-quality Si wafers, and last but not least availability of a native oxide for the material. It should be noted that using strained layers of SiGe in drain and source regions of *p*-channel MOS transistors has been pursued as one means to enhance carrier mobility, but for the most part CMOS is a homogeneous platform on Si. The younger field of microphotonics has meanwhile followed a different path in terms of the number of platforms developed for various needs.

Starting with the invention of gallium-arsenide (GaAs) "homojunction" lasers in 1962 [1], the structures used for semiconductor lasers (perhaps the most important integrated photonic device next to photodetectors) evolved into double-heterostructures [2, 3] for room-temperature operation in 1977 [4], and later to quantum-confined structures for higher performance at room temperature in 1978 [5]. However, not a single direct-bandgap material system is able to cover the wide optical spectrum range. For instance, GaAs and indium-phosphide (InP) and their ternary and quaternary alloys are used for different windows of telecommunication (telecom) infrared wavelengths of 750–1700 nm. Nitride semiconductors [indium gallium aluminum nitride (InGaAlN) alloys] span visible to ultraviolet wavelengths. In parallel, crystalline and amorphous dielectrics, such as quartz and silica, have been traditionally pursued in integrated optics for waveguides and other passive devices, while high-performance electrooptic (EO) modulators have been mostly fabricated on lithium niobate ($LiNbO_3$).

This balkanization of integrated photonics suggests that unfortunately no "magical" material or material system has been developed to date, whose unique collective properties can satisfy the somewhat orthogonal needs of the modern integrated photonics, including the choice of wavelength, efficient light emission and detection, large EO coefficient, strong optical nonlinear properties, ease of fabrication, integrability, scalability, reliability, inexpensiveness, etc.

2 Can silicon homogenize integrated photonics?

In the last quarter of century or so, silicon has been promoted and aggressively pursued as the elusive unifying material for integrated photonics. The field started by a series of seminal papers by R. A. Soref and coworkers [6–10]. The argued advantages of silicon over III–V OEICs have been the possibility of demonstrating much more compact optical waveguides with lower optical propagation loss, better processing yield, low cost and the potential compatibility with CMOS electronics. Several review papers [11–15] and books [16–20], have been written on silicon photonics, including some works by this author. For completeness, the basics of this exciting technology are briefly reviewed in the next paragraphs.

Figure 1 shows the idea of a silicon-based "superchip" [10]. Clearly, incorporating laser diodes, HBTs, HEMTs and BiCMOS devices on other materials are implicitly envisioned, i.e., the need for heterogeneous integration was acknowledged from the early days of silicon photonics. This vision is to a large extent in agreement with the state of the art, as seen throughout this paper. Figure 2 eloquently shows the importance and advantages of the versatile silicon-on-insulator (SOI) waveguide platform [11], which has been progressing rapidly since 1991 [21, 22]. The SOI platform has effectively become the benchmark platform for silicon photonics and several devices and photonic integrated circuits have been implemented on it since the mid-1990s [23–27]. The standard SOI waveguide technology is schematically represented later in the left structure of Figure 4. A thin film (220 nm to 3 μm) of silicon sits on top of a silicon dioxide (SiO_2) insulator layer, the so-called buried oxide or BOX, that serves as a lower-index bottom cladding layer for vertical optical confinement. The BOX layer is thick enough to prevent mode leakage into the silicon substrate. Techniques such as Separation by IMplantation of OXygen (SIMOX) process [28], or Bond and Etch-back SOI (BESOI) [29] can be employed to produce the wafers, but hydrogen implantation followed by thermal wafer splitting (the SmartCut™ process to produce Unibond® wafers [30]) has perhaps been the most successful approach to produce SOI wafers. An interesting review of these SOI wafer production methods can be found elsewhere [31].

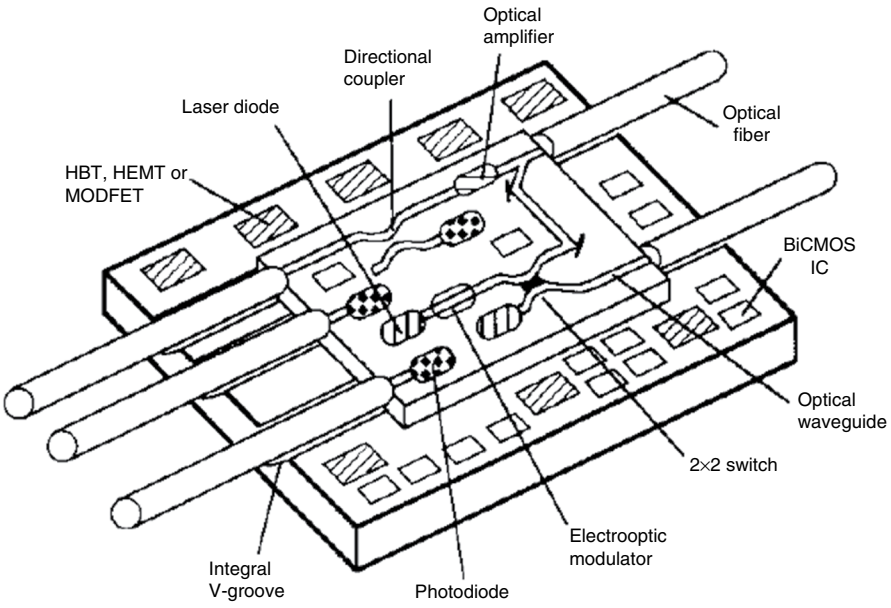

Figure 1 One of the original proposals for an optoelectronic integrated circuits on silicon [10], acknowledging the inevitable heterogeneous destiny of the technology.

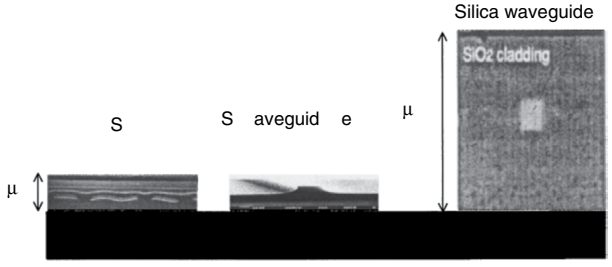

Figure 2 Advantage of the SOI waveguides in size compatibility with CMOS electronics, as opposed to silica waveguides [11].

A silicon-based solution for photonics would certainly be very rewarding and revolutionary. Hence, numerous researchers around the globe have been intensely working on advancing the field on various fronts with the ultimate hope of achieving a reliable technology that can be utilized as a universal platform for various optical functionalities and ultimately be integrated with microelectronic circuits monolithically on a single silicon chip. The endeavor has certainly been successful to the extent that a handful of companies have been marketing a variety of OEIC products for some years, most notably optical transceivers for data communications (datacom), Ethernet and other short-haul applications.

However, it was clear from the beginning that there is no "pure silicon" photonics, i.e., other materials are inevitably required. First, silicon does not absorb light at wavelengths above the material's bandgap (~1.1 μm). Instead, Ge or SiGe photodetectors have been employed, as reviewed in Section 3. Accordingly, it has been argued that group-IV photonics is a more accurate name than silicon photonics.

Second, the bandgap of bulk crystalline Si is indirect, i.e., the light emission process is phonon-mediated and the associated spontaneous recombination is very long, leading to a very low internal quantum efficiency [13, 32]. Consequently, achieving lasing in bulk Si has not been possible. Several approaches have been alternatively pursued. Unfortunately, for a variety of reasons, room-temperature electrically-injected silicon-based lasers remain elusive to date [13]. A pragmatic solution has been the hybridization of silicon photonic chips with III–V lasers, as reviewed in Section 4.

In reality and with the lack of any other practical solution, the silicon-photonic companies typically incorporate III–V lasers and germanium photodetectors, one way or the other, and silicon is mostly used for passive devices and modulators. For instance, Figure 3 shows a schematic of how one of Luxtera Corporation's early optical transceiver chips incorporates such non-silicon devices [33]. As depicted in Figure 4, it can be argued that "groups III-to-V" or "groups III-IV-V" photonics are semantically more accurate than silicon or group IV photonics for the established commercial technology. It is noted that the schematics of Figure 4 are very crude and generic and many variations exist, as seen throughout this paper. For instance, two cases for III–V monolithic

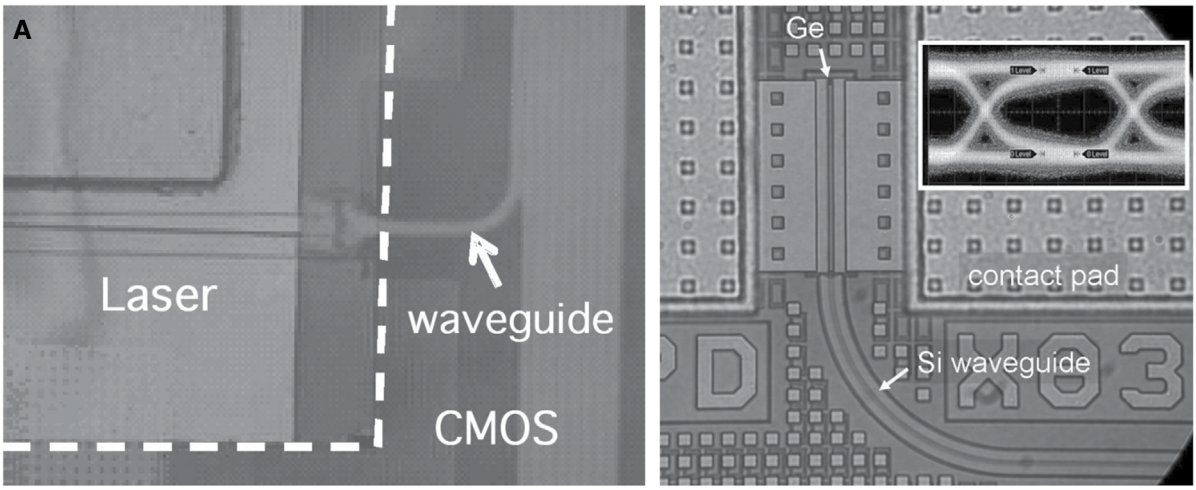

Figure 3 Images of optoelectronic chips produced by Luxtera Corporation and how (A) III–V lasers and (B) Ge photodetectros are integrated with Si waveguides [33].

integration is shown with respective pros and cons described in Section 4.

Third, despite a lot of effort for using crystalline silicon as an active region because of its high third-order optical nonlinearities, the omnipresent optical loss induced by two-photon- and free-carrier absorptions (TPA and FCA) has been very problematic [13, 34, 35]. Using thin films of other nonlinear materials "hybridized" on silicon substrates has been chipping away another core prospect of the SOI platform. These heterogeneous platforms for third-order nonlinear applications are reviewed in Section 5.

Fourth, although silicon optical modulators operating based on the free-carrier plasma effect have come a long way and their performance has been steadily improving, the inherent tradeoff between modulation bandwidth and depth remains a challenge and the devices cannot compete with telecom EO modulators in this regard. Hybridization of thin films of other materials known for their strong EO effect, e.g., $LiNbO_3$, on silicon substrates could be a possible route forward. Such materials also possess strong second-order optical nonlinearity and may enable compact chips for entangled photon generation and other quantum-optic-related applications. Efforts on such materials are reviewed in Section 6.

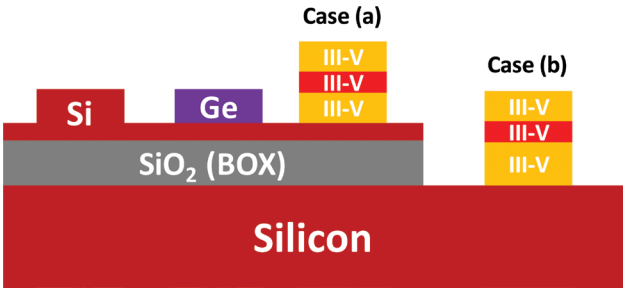

Figure 4 Simple schematic of the SOI waveguide platform, and how germanium and III–V compound semiconductor layers ought to typically be integrated in order to achieve hybrid photodetectors and lasers, respectively, suggesting that in reality there exists no pure silicon or even group IV photonics, rather "groups III-to-V photonics" or "groups III-IV-V photonics" are semantically more accurate.

Fifth, silicon is an ideal material for nonlinear integrated optics at wavelengths above ~2.2 μm. That is, the wavelength range in which TPA vanishes and the material becomes transparent even at high optical intensities, until multiphonon absorption kicks in and the loss increases again above ~6.5 μm. The 2.2–6.5 μm window covers the longer portion of the traditionally-defined short-wavelength infrared (SWIR of 1.4–3.0 μm) range as well as the shorter portion of the mid-wavelength infrared (MWIR of 3.0–8.0 μm). Using silicon for integrable devices in the atmospheric window of 3–5 μm, and sometimes the wider 2.2–6.5 μm range, has been loosely defined as mid-infrared (or mid-IR) silicon photonics. However, the BOX layer of the standard SOI technology is lossy across most of this range and hence other heterogeneous platforms such as silicon-on-sapphire, silicon-on-nitride, and air-clad waveguides have been developed, as reviewed in Section 7.

All in all, with the lack of any integrated optical material system for a whole range of applications, researchers have been reluctantly accepting that, despite their challenges and disadvantages, heterogeneous platforms appear to be the practical way forward. Still, silicon remains one of the most attractive substrate materials due to its low-cost, availability of large wafers, ease of handling and thermal

cycling, and well-established processing techniques, as well as possibility of integrating with CMOS electronics. The philosophy is to use silicon as much as possible but hybridize it with other materials when better performance can justify the challenges of hybridization.

3 Germanium photodetectors on silicon

As mentioned in the Introduction, the least controversial shortcoming of the benchmark SOI platform is its incapability of absorbing photons with $\lambda > \sim 1.1$ μm. For the O- to U-bands of telecom wavelengths (1.26–1.67 μm), Germanium's cutoff wavelength of ~1.8 μm appeals as a perfect choice. Ge-on-Si photodetectors have been in the making for three decades [36–51].

The challenge has been the material's large lattice mismatch with silicon (~4%). Thick Ge layers would lead to surface roughness, threading dislocations and increased dark photocurrent. Also, Ge does not have a stable oxide and passivating it to avoid surface recombination – which further increases the dark current – is another challenge. Dislocations can be controlled by graded SiGe buffered layers or in thin strained layers, both of which can reduce the dark current. Waveguide photodiodes with thin strained Ge layers on Si are more appealing for integrated chips. The small waveguide dimensions also result in shorter carrier transit time and increased detection bandwidth. The tradeoff is the length of the devices, that can be tens of micrometers long in order to increase the responsivity. One of the lowest reported dark current densities is ~40 mA/cm^2, achieved in a 1.3-μm-wide and 4-μm-long waveguide at – 1 V of bias [51]. The corresponding responsivity and 3-dB bandwidth are 0.8 A/W and 45 GHz, respectively. Evidently and despite all the efforts, relatively high dark current remains a disadvantage for Ge-on-Si waveguide photodetectors as compared with normal-incidence counterparts and III–V detectors.

To highlight the fabrication challenges of heterogeneous integration of Ge on Si substrates, the processing steps of one of the earlier high-speed photodetectors (40 Gb/s) by Intel Corporation is presented here [44]. Figure 5 shows schematics of the device, how it is integrated with a SOI waveguide, and its lateral cross-section. The following processing steps were conducted in the selected region where the photodetector was intended to be fabricated: (a) implanting the substrate with boron to reduce parasitic capacitance; (b) oxide deposition and patterning for defining the Ge region; (c) selective epitaxial growth of 1.3-μm-thick Ge; (d) chemical-mechanical polishing (CMP) of ~0.5 μm of the grown Ge; (e) thermal annealing to reduce the threading dislocation density; (f) *n*-doping of the Ge layer; (g) selective excess p^{++}-doping of silicon for improved ohmic contacts; (h) dopant activation by rapid thermal annealing; (i) metallization and patterning to form the diode contacts.

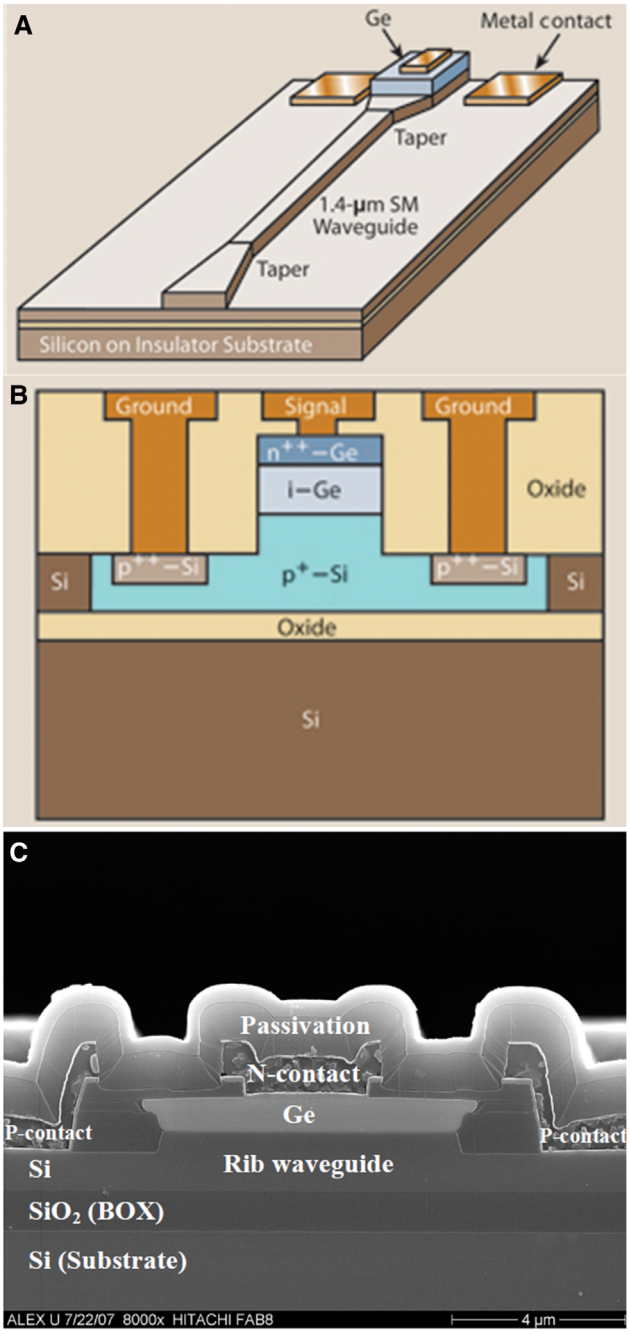

Figure 5 (A) Side-view, (B) cross-section and (C) micrograph of one of the early high-speed Ge waveguide photodiodes developed at Intel Corporation [44].

The extra steps for Ge hybridization are the selective epitaxial growth, CMP, and thermal annealing. Such extra, sometimes complicated, fabrication steps are typically the price tag for any heterogeneous technology, more examples of which are discussed in this paper. Meanwhile, one advantage of Ge, over other materials to be discussed, is that, despite its large lattice mismatch, thin films of it can be epitaxially grown on Si with little complications. Not all other materials can be as easily grown on Si, and hence other heterogeneous integration techniques, such as wafer- and flip-chip-bonding, ought to be devised as seen in the following sections.

4 III–V Lasers on silicon

Attaining lasing is perhaps the holy grail of silicon photonics. Unlike compound semiconductors, bulk crystalline Si is an indirect bandgap material and light emission is mediated by phonon emission or absorption. This second-order emission process is very weak (with an internal quantum efficiency of ~10^{-6}) and the spontaneous recombination lifetime is in the millisecond range [13]. In principle, silicon can provide high material gain at high carrier injection levels for lasing. However at high injection levels, FCA and Auger recombination prevent achieving any net optical gain [13, 32].

Since the early 1990s, several approaches have been pursued to increase the quantum efficiency of luminescence in bulk Si. They include, but not limited to, Erbium (Er)-doped Si, Si-rich oxide or Si nanocrystals (NCs), Er-doped Si NCs, deposition of boron dopant with SiO_2 nanoparticles mix on Si, surface texturing, dislocation loops, and stimulated Raman scattering. However, for a range of specific reasons beyond the scope of this paper and reviewed elsewhere by B. Jalali and this author in 2006 [13], unfortunately none of these approaches have been able to offer room-temperature electrically-injected lasers. Since then, an interesting development has been room-temperature lasing in strained, *n*-type-doped Ge on Si [52]. Strain makes Ge an "almost" direct bandgap material and *n*-doping populates the engineered direct conduction band. Evidence of room-temperature electrically-injected lasers at a high doping level of 4×10^{19} cm^{-3} and tensile strain of about 0.2% in the 1520–1700 nm range was reported in 2012 [52]. However, a high optical loss of 90 cm^{-1}, induced by high doping levels right in the middle of the active region of the waveguides, results in high threshold currents and the approach does not appear to be ready for prime-time applications yet. Another recent photonic material development has been germanium tin (GeSn), a group IV binary compound semiconductor alloy with direct band-gap below 0.8 eV at certain compositions. No GeSn laser has been demonstrated yet, but electroluminescence devices spanning ~1530–1900 nm wavelengths have been reported [53].

The disappointing reality of the lack of a viable approach for achieving Si-based lasers has not affected the attractiveness of silicon photonics. Instead, hybrid and heterogeneous approaches have been aggressively pursued. The most straightforward hybrid approach that comes to mind is to flip-chip bond or solder-based assemble a completely grown and processed functional III–V laser onto the silicon photonic circuit and couple the laser output into silicon waveguides via some coupling mechanism. These approaches are indeed as old as silicon photonics itself [54–57]. Variations of this approach are fairly established and adopted by the silicon photonic industry, e.g., Luxtera Corporation [33, 58], NEC Corporation [59], Toshiba Corporation [60], and Fujitsu Laboratories [61]. Perhaps such more straightforward per-device flip-chip bonding approaches suffice the present low-volume, low-throughput needs of the industry but for future high-volume demanding markets, heterogeneous monolithic integration of III–V wafers and Si wafers, or already processed circuits, is more desirable.

Epitaxial growth of III–V heterostructures on Si substrates has been pursued for over 25 years [62]. Similar to Ge-on-Si epitaxial growth, however, the challenge is the large lattice mismatch (4.1%) between GaAs and Si, as well as 250% difference of their thermal expansion coefficients. Direct growth of GaAs-based heterostructures on Si creates very high densities of surface misfit dislocations (~10^9 cm^{-2}), which transform into threading dislocations propagating into the active region of lasers during the growth. Consequently, the lasers have very short lifetime caused by catastrophic failure. It turns out that the lattice mismatch of Ge and GaAs is very small (0.077%) and their thermal expansion coefficients match over large temperature ranges. Hence, the same graded SiGe epitaxial growth technology discussed for SiGe photodetectors can be utilized as buffer layers in order to achieve low-dislocation GaAs-based epilayers on Si. A challenge has been the growth of a polar (GaAs) over a nonpolar (Si) surface, a phenomenon long known as antiphase disorder [63]. Certain substrate preparation and initial growth precautions can significantly alleviate the issue [64–67]. AlGaAs/GaAs quantum well lasers on relaxed SiGe buffers layers on Si have been reported [68]. Surface threading dislocation densities were as low as 2×10^6 cm^{-2} allowing continuous-wave, room-temperature lasing at a wavelength of

858 nm. Yet, relatively low differential quantum efficiency of 0.24 and high threshold current density of 577 A/cm^2 impaired the devices.

Similarly, other approaches for growing GaAs-based laser on Si, including strained-layer superlattices (SLS) [69, 70] and more recently quantum dot dislocation filters (see Figure 6A) [71, 72], typically suffer from high threshold current and short lifetimes. At any rate, GaAs-based lasers, even their longer-wavelength quantum-dot types, become increasingly less efficient light emitters at wavelengths above silicon's bandgap, and InP-based lasers are more suitable for integrating with Si and for telecom wavelengths. In addition to the thermal expansion coefficient difference and polar/nonpolar antiphase disorder issues, the problem with direct InP growth on Si is the even larger (8.1%) lattice mismatch between the materials, prohibiting using graded SiGe buffers. Even employing InGaAs SLS buffer layers is not as effective as in GaAs. Initial works resulted in high dislocations densities in the order of 10^8–10^9 cm^{-2} [76]. Progress was later made for this method [77–79], yet the dislocation densities remain in the 10^7 cm^{-2} range, which is an order of magnitude higher than lattice-matched growth. A somewhat radical solution for direct growth of III–V lasers emitting in the 1550-nm telecom wavelength is using another material system, e.g., gallium antimonide (GaSb)-based lasers. Strained GaInSb/AlGaAsSb quantum-well lasers have been grown on Si, but at room temperature the devices could operate only under pulsed bias and with a high threshold current density of 5 kA.cm^{-2} [80].

The tough circumstances may leave no option other than relying on some bonding techniques. As discussed, a very practical, yet low-yield and high-cost, approach is flip-chip bonding of completely processed individual lasers on silicon photonic chips. A more monolithic approach for large-scale integration is to first conduct wafer (full or partial) or die bonding of III–V epilayers onto silicon photonic chips, followed by processing the III–V devices. An advantage is that aligning III–V devices with Si waveguides during lithography is typically easier this way than during chip bonding or assembly.

Indirect bonding methods, including adhesive (e.g., based on polymers) and eutectic bonding (based on metals such as In-Au and Pb) may be convenient ways to effectively "glue" the two wafers. However, bonding by polymer materials, such as the benzocyclobutene (BCB) family [81], may be fine for lab demonstration but is not reliable for practical applications due to weak formed

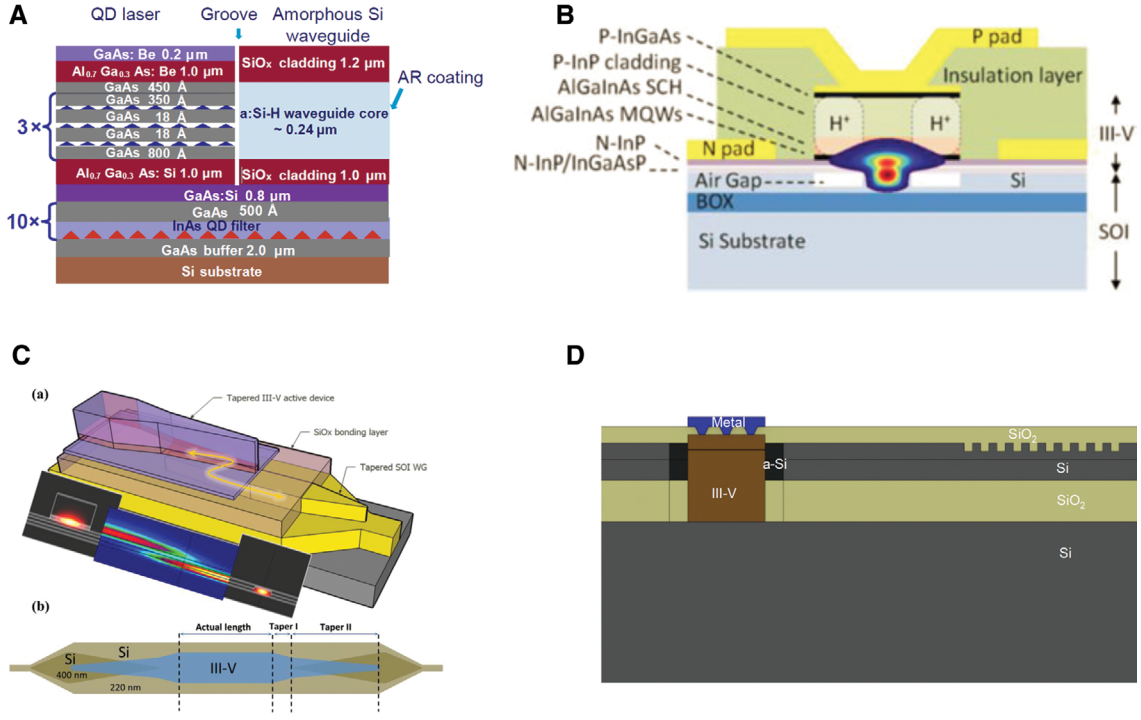

Figure 6 Schematics of four heterogeneous approaches to integrate III–V laser on Si substrates: (A) monolithic epitaxial growth of InGaAs/GaAs quantum-dot regions buffered by 10 layers of inactive dots to filter propagation of threading dislocations into the active region [72]; (B) evanescently-coupled InP lasers bonded on SOI waveguides [73]; (C) tape-waveguide vertical coupling form III–V gain regions into SOI [74]; and (d) bonding III–V gain regions into trenches made in silicon for planar coupling between the two [75].

bonds. Also, metallic layers of eutectic bonding cause optical loss.

A more reliable approach is direct wafer (or fusion) bonding of InP and Si layers. The idea can be traced back to Lord Rayleigh [82], who bonded optically-polished glass plates at room temperature. In modern semiconductor processing, two atomically smooth (<1 nm roughness) and clean surfaces are brought to physical contact at low temperatures (to form atomic bonds with no worry of the lattice-mismatch hurdle) and subsequently the bonds are strengthened by thermal annealing. The research in this area was motivated by bonding two Si wafers in the 1980s for electronic applications, pioneered by researchers at IBM [29] and Toshiba [83]. Interestingly, Ref. [29] reports one of the very first SOI wafers achieved by the aforementioned bonding and etch-back technique.

Taking advantage of hydrophilic surfaces (e.g., SiO_2) or assisting the process by oxygen plasma can enhance the initial bonding, as follows. One of the earliest III–V lasers bonded to Si wafers is by C. Seassal et al. [84], with Ecole Centrale de Lyon and LETI-CEA in France, where they managed to demonstrate optically-pumped InP microdisk lasers bonded to Si wafers. Two SiO_2 layer were formed by plasma-enhanced chemical vapor deposition (PECVD) on both InP and Si wafers, and then polished, cleaned, bonded and annealed at 200°C for 60 minutes to increase the bonding strength. The InP substrate was subsequently removed by selective wet etching using an $In_{0.53}Ga_{0.47}As$ sacrificial (etch-stop) layer, exposing the heterolayers for microdisk laser processing, i.e., 6-μm diameter disks were patterned by standard dry etching techniques. An electrically-injected InAsP/InGaAsP microdisk laser was later demonstrated [85]. One issue with this approach is the quality of the PECVD oxide and the strength of the created bonds and their stability at elevated temperatures [86]. Low heat dissipation of the underlying dielectric SiO_2 layer [see case (a) in Figure 4], leading to degraded laser performance, is another disadvantage of using hydrophilic SiO_2 bonding layers.

One challenge for wafer-bonding approaches is how to couple light into Si waveguides. Based on the concept of vertical coupling via evanescent coupling (originally proposed and demonstrated in the context of III–V microdisk lasers stacked on another III–V bus waveguide [87]), the mentioned French research groups managed to couple light from optically-pumped microdisk lasers into silicon strip waveguides by decreasing the total SiO_2-SiO_2 hydrophilic surfaces from 800 nm down to 300 nm [88].

Pioneered by a group at Uppsala University, Sweden, plasma-assisted direct bonding of semiconductors has been shown to be an interesting technique to avoid SiO_2 hydrophilic layers and their complications [86, 89–91]. Based on this bonding technique, researchers at the University of California, Santa Barbara (UCSB), demonstrated optically-pumped [92] and later the first electrically-injected [93] evanescently-coupled edge-emitting Fabry-Perot AlGaInAs/InP lasers coupled into Si waveguides (see Figure 6B). A hybrid optical mode, mostly residing in the SOI waveguide, has partial overlap with the laser separate confinement structure, allowing coupling between the two modes. Since then and in collaboration with Intel Corporation, the UCSB group has impressively matured this platform and managed to demonstrate more complicated photonic circuitry, i.e., demonstrate and integrate lasers [including Fabry-Perot, microdisk, microring and distributed Bragg reflector (DBR) types], semiconductor optical amplifiers, electroabsorption and phase modulators, as well as photodetectors. Detailed reviews of these works can be found elsewhere [73, 94]. Also, other researchers have shown very similar lasers with InGaAsP, rather than AlGaInAs, multi-quantum well active regions [95].

Meanwhile, arguing that the evanescently-coupled lasers should better have more confinement in the InP-based gain region than the Si waveguides, research groups at Ghent University and IMEC, Belgium, in collaboration with the mentioned French groups, demonstrated somewhat different electrically-pumped evanescently-coupled lasers [96]. Another approach pursued by the same groups is using III–V gain regions and distributed reflectors on SOI waveguides linked by tapered adiabatic mode converters for realizing tunable lasers (see Figure 6C) [74, 97]. Finally, Skorpios Technologies has envisioned and developed a planar platform in which unprocessed III–V epilayers are metal-bonded into grooves made in silicon substrate, such that the processed laser is eventually butt-coupled into SOI waveguides [75] (see case (b) in Figure 4 and Figure 6D). This approach avoids the inherent shortcoming of vertically-coupled lasers in terms of guided optical mode distribution between Si and InP waveguides and offers efficient direct optical coupling between the two planar (horizontally-aligned) regions. Other advantages include better heat dissipation due to the omission of the BOX underneath the laser, allowing laser operation up to 80°C, as well as hermetically sealing the lasers in SiO_2 encapsulation, eliminating the need for their packaging.

To summarize this Section, it is apparent that any existing and perhaps upcoming laser technology on Si has its own pros and cons. Thus, it is hard to judge which of so many reviewed competing approaches will prevail. But it is likely that some heterogeneous integration methods, based on III–V lasers pre- or post-process bonded to Si, will be the most relevant solutions in the foreseeable

future. Figure 6 summarize results from some of the key such hybrid laser approaches by the various groups discussed above.

5 Third-order nonlinear photonics on silicon

Silicon has a centrosymmetric lattice structure, thus it inherently lacks second-order optical nonlinearity. It has high third-order optical nonlinearity (both Kerr and Raman types), though. Specifically, silicon waveguides have a much high nonlinear parameter $\gamma=(\omega\times n_2)/(c\times A_{eff})$ compared to traditional integrated-optics platforms, e.g., silica fibers or planar waveguides. Here, n_2 is the nonlinear refractive index, λ and ω are the wavelength and angular frequency of light, respectively, and c is the speed of light in vacuum. From the early 2000s, pioneered by B. Jalali's group at UCLA, both Raman-based [98–103] and Kerr-based [104, 105] nonlinear effects have been explored in silicon photonics. Numerous studies have been published in the area of nonlinear silicon photonics by several groups, reviews of which can be found elsewhere [13, 106]. An omnipresent problem in the telecommunication wavelengths, however, is the TPA at required high optical intensities and the even higher FCA induced by it [13, 34, 35]. Certain approaches can reduce the carrier lifetime, alleviate the problem and modestly improve the nonlinear device performances. Active carrier sweep-out in reverse-biased waveguide diodes has been proposed [35] and demonstrated [107]. This author and coworkers demonstrated energy harvesting based on two-photon photovoltaic effect to achieve energy-efficient nonlinear devices [108–112]. Nonetheless, in all of these sweep-out-based solutions, the carrier lifetime remains relatively high and FCA cannot be significantly subdued due to free-carrier screening of the junction electric field [113]. Difficulties of coupling light into higher order modes of specially-designed waveguides notwithstanding, cladding pumping of nonlinear silicon photonic devices is another potential solution [114]. Also, introducing midgap states through high-energy irradiation of ions, e.g., helium, is another means of modestly reducing the carrier lifetime, although it comes at the expense of higher linear propagation loss. Therefore, only small values of net gain in Raman amplifiers has been observed [115].

Several researchers have totally moved to other nonlinear materials such as hydrogenated amorphous silicon (a-Si:H) [116–118], silicon nitride (SiN) [119–121], Hydex™ [122, 123], chalcogenide glass [124–126], and tantalum pentoxide (Ta_2O_5) [127–132] waveguides on silicon substrates to totally circumvent the nonlinear loss problem of SOI waveguides. The argument is that the improved nonlinear figure of merit, FOM=$n_2/(\beta_{TPA}\times\lambda)$ in these materials – with negligible TPA coefficient, β_{TPA} – is more important than the previously argued high γ of Si. The common idea for all of these heterogeneous platforms is to use deposition, spinning or other methods of thin film formation to create waveguides on a dielectric bottom cladding layer (usually SiO_2) on Si substrates and exploit the materials' nonlinear optical properties for functions such as supercontinuum generation, four-wave mixing, self-phase modulation, cross-phase modulation, third-harmonic generation, stimulated Raman scattering, etc. To give an example of such materials, a novel platform based on Ta_2O_5 developed at the author's lab at CREOL is reviewed in the following [131, 132].

Table 1 summarizes n_2 and β_{TPA} in all the materials discussed in the previous paragraph in comparison to SiO_2, as a benchmark. The literature of a-Si:H is inconsistent and seemingly is very dependent on the deposition condition, but very high values of n_2 have been claimed [116, 118]. However, a tradeoff between n_2 and β_{TPA} is observable and overall the considerable value of β_{TPA} (which can be much higher than crystalline Si [116]) limits the FOM (e.g., ~5 in Ref. [118]). The other materials of interest in Table 1 have negligible β_{TPA} and hence measuredly or potentially possess very high FOM. Among them, Ta_2O_5 has an n_2 three times higher than SiN and comparable to chalcogenide glasses. Meanwhile, its refractive index of ~2.1 is higher than Hydex's (~1.7) and its damage threshold is much higher than that of chalcogenide glasses. The reduction of the waveguide dimensions in the low-loss Ta_2O_5 submicron waveguide fabrication technique described below reduces A_{eff}. Consequently, the γ of Ta_2O_5 waveguides can be much higher than the competing materials of Table 1.

Sputtering and standard lithography and reactive ion etching processes have been previously used to form Ta_2O_5 waveguides [128, 130]. However, sputtered waveguides

Table 1 Nonlinear refractive indices and two-photon absorption coefficients of various materials [116, 118, 121, 126, 127, 133].

Material	n_2 ($\times10^{-20}$ m^2/W)	β_{TPA} (cm/GW)
SiO_2	3.2	Negligible
Hydex	11	Negligible
SiN	26	Negligible
Ta_2O_5	72.3	Negligible
Chalcogenide	~100	6.2×10^{-4}
Crystalline Si	250	0.7
a-Si:H	2100–4200	0.25–4.1

suffer from high propagation loss, e.g., as high as 8.5 dB/cm in 18-μm-wide waveguides [130]. Also, compact (submicron) Ta_2O_5 waveguide are not easily feasible based on such conventional schemes. Based on our proposed scheme, called selective oxidation of the refractory metal (SORM) Tantalum (Ta), we have recently demonstrated the first high-index contrast Ta_2O_5 submicron waveguides and microring resonators on Si substrates (see Figure 7) [131, 132].

The improved fabrication process of Ref. [132] starts with sputtering Ta, rather than Ta_2O_5, and making stripes out of the refractory metal by electron-beam lithography and chlorine-based selective etching. The etching recipe is highly selective on Ta over the photoresist, allowing smooth sidewalls and hence low propagation loss. The Ta stripes are consequently oxidized to form Ta_2O_5 channel waveguides. Ridge waveguides can be easily achieved too by two iterations of Ta sputtering, the first of which is fully oxidized to form a Ta_2O_5 slab region. Waveguides with propagation loss of 4.9 dB/cm, microring resonators with loaded quality factor of 6×10^4 and grating couplers for convenient in- and out-coupling are demonstrated. Figure 7 summarizes some of the demonstrated waveguide properties [132]. These demonstrations suggest that Ta_2O_5-on-Si is potentially a viable platform for high-performance nonlinear integrated photonic applications.

6 Second-order nonlinear photonics on silicon

There have been some reports on breaking the lattice symmetry of bulk Si by applying stress on Si waveguides to take advantage of the induced second-order optical nonlinearity as well as linear EO (or Pockels) effect [134–136].

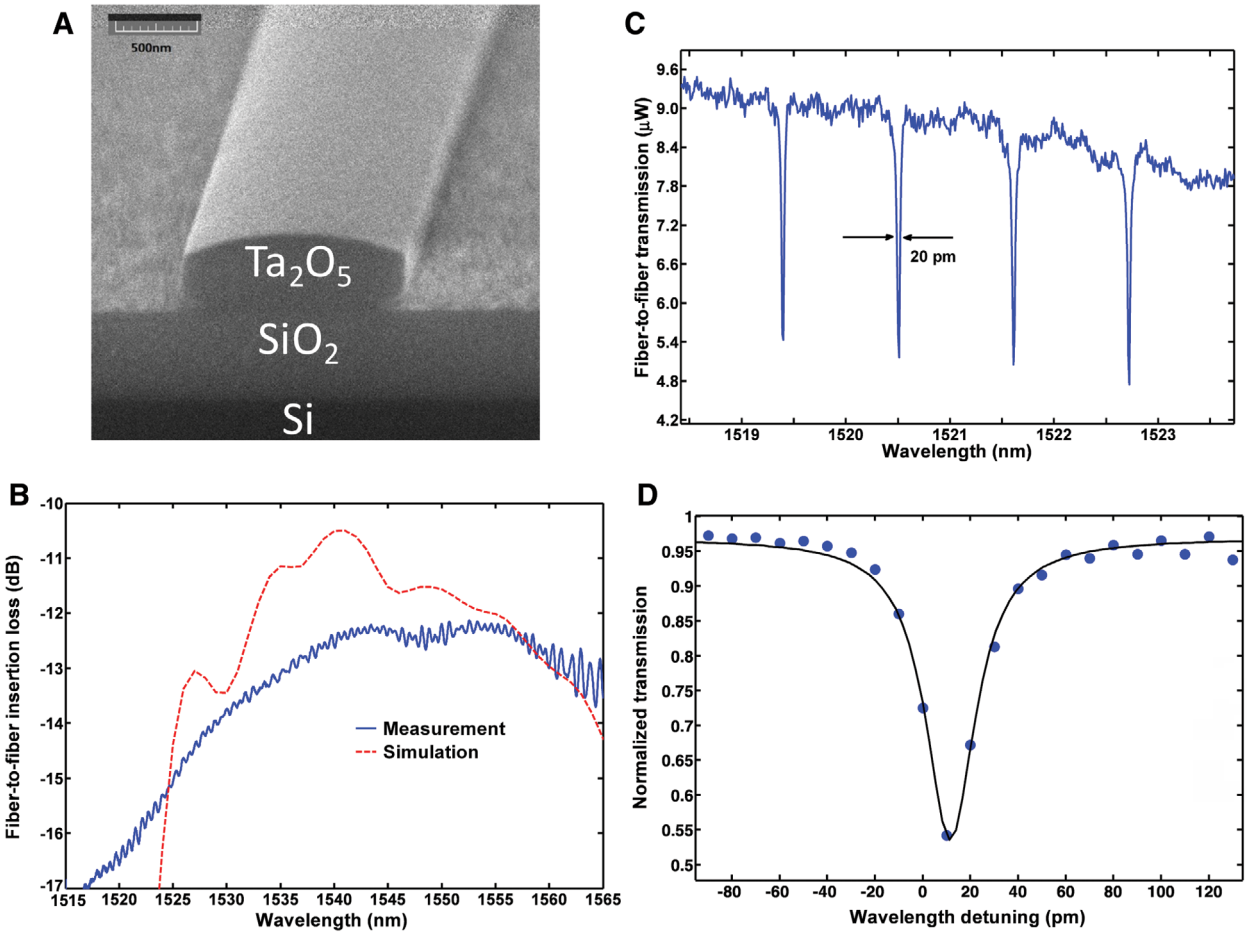

Figure 7 (A) Microigraph of Ta_2O_5 waveguides on Si; (B) measured and simulated transmission spectrum of grating couplers on the platform; (C) measured spectral response of the microring resonators fabricated on the platform in the 1550 nm range; (D) zoomed version of one of the resonances in (C), also showing fitted data to it [132].

In this respect, this author and coworkers have been able to induce electronically-tunable birefringence in SOI waveguides by blanketing them with a piezoelectric transducer made of lead zirconium titanate (PZT) [137, 138]. However, the amount of induced birefringence is in the range of 3×10^{-5}, which is large enough for electrically tuning the phase-mismatch of transverse-electric (TE) and transverse-magnetic (TM) modes in parametric nonlinear optical effects, but not enough to take advantage of the effect for second-order nonlinear effect itself. It is true that the induced strain can be higher using stressed cladding layers, such as SiN, and in smaller waveguide cross-sections [134–136], but overall the extent to which second-order optical nonlinearity and/or Pockels effect can be induced by such methods is questionable considering that single-element Si is a nonpolar crystal.

As far as optical modulation function in silicon photonics is concerned, the free-carrier plasma effect was proposed in the early works by Soref et al. [8–10] as a viable alternative to the Pockels effect. In essence, carrier injection, depletion or accumulation in *p-n* junction diodes or MOS capacitors, typically incorporated into Mach-Zehnder interferometers (MZI) or microrings, can be used to modulate the refractive index or optical loss. Numerous works on such modulators have been reported, a review of which can be found elsewhere [139]. Although Si optical modulators with adequately high bit rate (~50 Gb/s) and low half-voltage length-product $V_\pi.L$ (~2.8 V.cm) have been reported in MZIs, the devices only offer modest (3–5.5 dB) of modulation depth or extinction ratio [140, 141]. Such low modulation depth may be enough for near-term very short-haul links but this certainly remains a shortcoming for the long-term requirements of the industry, where at least 7 dB of modulation depth at high speeds is demanded [139]. Indeed, the modulation depth times the bit rate may be a better figure of merit, which is ~150 to ~280 dB.Gbs^{-1} in the mentioned state of the art works [140, 141]. In clear contrast, the benchmark $LiNbO_3$ modulators boast 20 dB or better modulation depth (the industry standard for digital communications) [142] and 40 Gb/s or higher bit rates are commonplace in commercial long-haul telecom systems, giving a figure of merit of at least 800 dB.Gbs^{-1}. Up to 100 GHz modulation bandwidth has been measured in $LiNbO_3$ with careful RF design of traveling-wave electrodes as early as 1998 [143], hence even higher modulation depth times bit rates are feasible in principle, the complications of detection and electronic circuitry for modulation and detection notwithstanding.

It again appears that heterogeneous integration of Si with another material with strong second-order optical nonlinearity, as well as linear EO or electro-absorption (EA) effect, may be the way forward. Nitride semiconductors have high second-order nonlinearities. GaN has been bonded to Si by PECVD SiO_2 with measured second-order nonlinear susceptibility, $\chi^{(2)}$, of ~16 pm/V [144]. However, as mentioned in Section 4, the quality of PECVD oxide is low for bonding. Also, the uniformity of the thin GaN films obtained by CMP, after removing the (111) Si substrate, on which they were originally grown, is an issue. Sputtering of AlN on Si wafers coated with SiO_2 has also been reported [145]. However, the crystalline quality of sputtered AlN is expectedly low, leading to a weak $\chi^{(2)}$ of ~4 pm/V. Nonlinear polymer materials have shown strong EO effect and, their long-term reliability notwithstanding, have potential for high-performance modulators in Si waveguides coated with them [146].

Telecom wavelengths are far from silicon's bandgap. Hence, EA modulators based on the Franz-Keldysh effect (FKE) are not possible on Si. But both the quantum-confined Stark effect (QCSE) and FKE in SiGe can be exploited at longer wavelengths. $Si_{0.6}Ge_{0.4}$-Si quantum-well waveguide EA modulators based on QCSE operating at 1.15 μm wavelength were demonstrated at the University of Michigan in 1998 [147]. Later, another team employed Ge-$Si_{0.1}Ge_{0.9}$ quantum wells in surface-illuminated modulators to red-shift the operating wavelength to ~1.45 μm [148]. More recently, GeSi, i.e., Ge epitaxial layer comprising <1% of silicon, has been used to exhibit strong FKE around 1.55 μm and demonstrate EA modulators with 10 dB extinction ratio [149]. Mellanox Technologies has been recently maturing this technology to integrate it into their OEICs [150]. Another approach, pursued at UCSB, is to take advantage of the quantum-well intermixing technique in order to shift the bandgap of InP-based heterostructures and achieve EA modulators on the same elipayers used for lasers in a hybrid OEIC on Si substrates [73].

An alternative approach pursued at the author's group at CREOL is heterogeneous integration of $LiNbO_3$ on Si [151]. With high nonlinear optical coefficients (e.g., $d_{33}\approx$-25.2 pm/V), $LiNbO_3$ is an ideal material for nonlinear integrated photonics. Also, single-crystalline $LiNbO_3$ has large EO coefficients ($r_{33}=\approx$31 pm/V and r_{13}=8 pm/V) and a wide transparency range (0.4–5 μm wavelength) [152]. Indeed, standard $LiNbO_3$ waveguides are widely regarded as the best vehicle for EO modulation in the photonic industry [142] with impressively high modulation bandwidths (over 100 GHz [143]). As mentioned before, $LiNbO_3$ modulators undoubtedly offer higher performance (in terms of modulation bandwidth and modulation depth) compared to Si-based optical modulators.

$LiNbO_3$ waveguides are traditionally formed by diffusion of titanium, the process of annealed proton exchange

or implantation of dopants (e.g., oxygen ions) in bulk wafers [142]. Any of these processes can only slightly alter the refractive index of the material, i.e., the index contrast of the obtained stripe waveguides is rather small (0.1–0.2) and hence the guided modes are weakly confined. In EO modulators, this shortcoming leads to large device cross-sections (widths of several microns) and consequently large $V_\pi.L$ of 10–20 V.cm depending on modulation frequency and characteristic impedance [143, 153]. Indeed, for current very high-speed applications, the frequency response of $LiNbO_3$ modulators is limited by the long lengths of the electrodes, thus using travelling-wave electrodes becomes essential [142, 143]. Large cross-section waveguides also imply the need for high-power sources to achieve high optical density for the onset of optically-induced $\chi^{(2)}$ nonlinearity. Furthermore, for weakly-confined waveguides the bending loss becomes significantly high for small radii. Consequently, the possibility of integrating several of the devices on the same chip for advanced vector modulation formats, e.g., quadrature amplitude modulation (QAM), becomes difficult and cost-prohibitive when the number of MZIs exceeds a few. Monolithic integration of only four $LiNbO_3$ MZIs for 16-level QAM modulation with a large module size of $90\times13.5\times7$ mm^3 is the state of the art [154].

Achieving thin films of $LiNbO_3$ on a material like SiO_2 with much lower index and a method for submicron ridge or channel formation (instead of the traditional stripe type) can potentially alleviate the discussed problems and yield high-contrast submicron waveguides. However, fabrication of high-quality thin films single-crystalline form of $LiNbO_3$ has been proven to be very challenging. Chemical vapor deposition [155], sol-gel processing [156], RF sputtering [157–159], and pulsed-laser deposition [160, 161] have been pursued with little success. That is, the films obtained by any of these methods typically have low optical quality, i.e., the EO coefficients are much smaller (up to more than 10 times) than the mentioned bulk values.

Alternatively, crystal ion slicing has been successfully employed to obtain high-quality thin films of crystalline $LiNbO_3$ [162–165]. A combination of deep helium ion implantation, selective etching and epoxy-resin bonding has been applied to transfer 5-to-10-μm-thick $LiNbO_3$ layers to silicon substrates [162]. $LiNbO_3$-on-$LiNbO_3$ thin films and modulators, buffered by a SiO_2 layer, attained by ion implantation and wafer bonding have been also reported [163, 164]. Interestingly, the EO properties of the films was not degraded during the implantation process. However, the argon ion beam milling process employed to achieve ridge waveguides causes high propagation loss. In another report, the adhesive polymer BCB, was used instead for wafer bonding and demonstrate electrooptically tunable $LiNbO_3$-on-$LiNbO_3$ microring resonators [165]. Polymers, like epoxy-resin [162] or BCB [165], may be simple and straightforward solutions for lab demonstrations, but, as mentioned before, they are generally not reliable for practical applications due to the weak nature of the formed bonds.

The author's group has been able to address all the above challenges and for the first time demonstrate reliable $LiNbO_3$-on-Si thin films as well as low-loss waveguides, microring resonators and record-low $V_\pi.L$ modulators on them [151]. The highly repeatable and reliable process used for attaining thin films (400–500-nm thick) of $LiNbO_3$ on Si begins with ion implanting commercially available $LiNbO_3$ wafers to weaken bonds for future slicing. A standard silicon substrate is coated with a thermally-grown SiO_2 layer to be later employed as waveguide cladding layer. The use of thermally-grown SiO_2, rather than PECVD oxide, is critical in forming strong bonds. The two wafers are then bonded at room temperature, after which they are heated to 200°C to not only slice the $LiNbO_3$ wafer at the bonds weakened by ion implantation, but also to strengthen the formed bond at the $LiNbO_3$-SiO_2 interface. CMP is the last step applied on the bonded $LiNbO_3$ thin films to attain smooth surfaces for waveguide processing.

Another historic challenge for $LiNbO_3$ integrated photonics has been the difficulty of etching the material to produce waveguides with smooth sidewalls. Ion beam milling [164, 165], plasma etching [166, 167], and wet etching [168–171] are the main techniques pursued. Wet etching in particular has produced fairly low-loss waveguides [171]. However, slow etch rate, undercutting, asymmetric profiles and large feature sizes are common shortcomings of wet etching recipes and submicron waveguides cannot be achieved.

One solution is to guide light in SOI waveguides and bond a thin film of $LiNbO_3$ on top of the SOI chip. Both free-standing [172] and BCB-bonded films have been reported [173]. The shortcomings of this method is not only the instability of the free-standing structures and/or the unreliability of polymers but also the fact that only the evanescent tail of the SOI waveguide mode reaches out to the $LiNbO_3$ top cladding, leading to small (e.g., 11% [173]) overlap of the EO active region with the optical mode.

A novel approach proposed at CREOL is rib-loading $LiNbO_3$ slab waveguides with an index-matching material, such that most of the optical energy still resides in the slab region [151]. Coincidently, the index of Ta_2O_5 matches that of $LiNbO_3$ (~2.1). Hence, the same SORM technology described for attaining Ta_2O_5 waveguides on SiO_2-coated

Si [131, 132] can be applied on thin films of $LiNbO_3$ bonded to Si and readily achieve waveguides. Figure 8A and B show a surface-scanning micrograph (SEM) of a fabricated device as well as the device schematic and calculated optical mode [151]. Strong overlap of the optical field with the $LiNbO_3$ is evident in the simulated mode in Figure 8C. Figure 8D shows the modulation response of the devices at low frequencies. $V_\pi.L$ as low as 4 V-cm is obtained in push-pull configured MZI modulators. The reported $V_\pi.L$ is three times lower than the best commercial devices. Calculations show $V_\pi.L$ as low as 1.2 V-cm is possible. Preliminary high-speed characterization, using S_{21} parameter of a network analyzers, suggests operation up to 10 GHz. High-speed measurements based on travelling-waveguide electrodes for velocity matching of RF and optical waves are underway. A clear advantage of the results in Figure 8D is that the modulation depth is expectedly very high (~20 dB) and is a clear advantage over free-carrier modulated Si modulators. With fitting a sinusoidal function to the output of the MZIs, highly linear transmission (<3% error in the fitting) was extracted, confirming the devices' suitability for analog communications in addition to the more common digital data- and telecommunications. Finally, Figure 9 summarizes the improvement achieved by the presented approach in terms of waveguide effective area and minimum radii for negligible bending loss over conventional diffused waveguides and where it stands with respect to other integrated photonic platforms.

7 Mid-infrared integrated photonic platforms

Optics in the mid-wave infrared (MWIR or mid-IR) wavelengths, particularly the atmospheric transmission window of 3–5 µm, has been researched on for over 60 years [174]. Historically, mid-IR optics has been motivated by applications such as light detection and ranging (LIDAR) and infrared countermeasures. Over the past decade, mid-IR photonics has found a host of civilian applications, e.g., Fourier transform infrared (FTIR) spectroscopy, remote biological and chemical sensing for environmental monitoring and free-space optical communications [175–177]. More recently, clinical applications, like tissue photoablation, have also emerged [178–180]. These applications would have not been possible without successes in high-performance uncooled commercial mid-IR optical sources [181, 182] and photodetectors [183, 184]. However, most current systems are based on assemblage of discrete components, i.e., true integration is lacking. Device miniaturization and monolithic integration would hence be a great

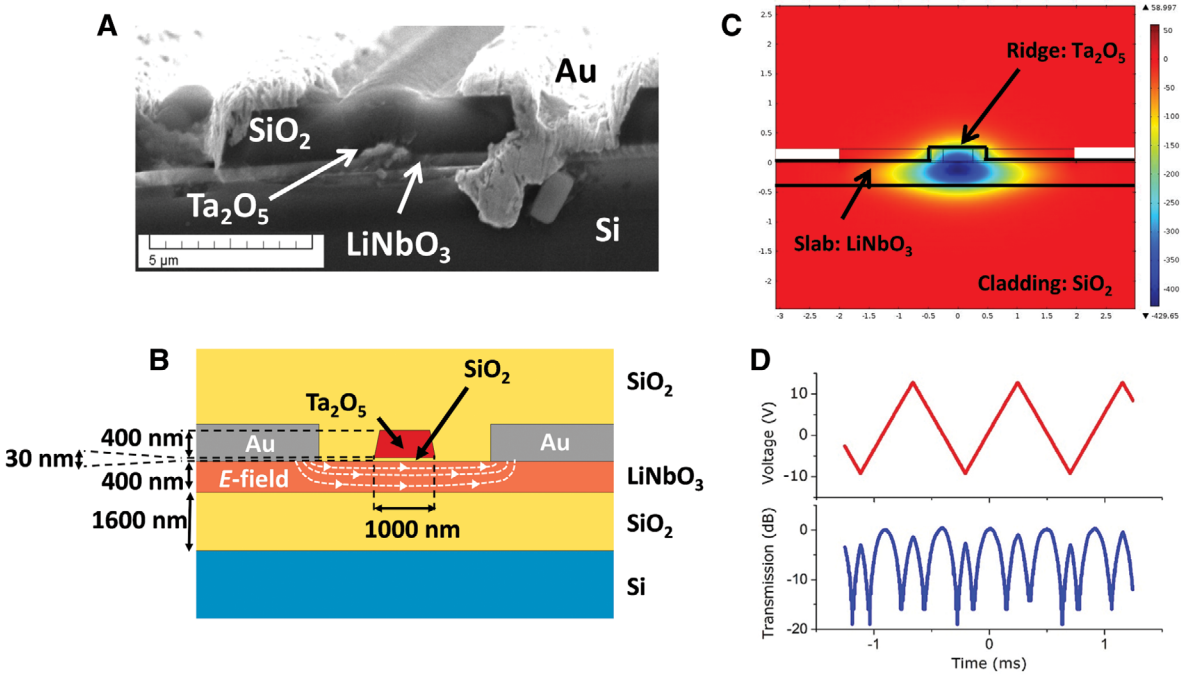

Figure 8 (A) Micrograph, (B) schematic, (C) optical mode simulation and (D) measured modulation response of the first demonstrated $LiNbO_3$-on-Si modulators [151].

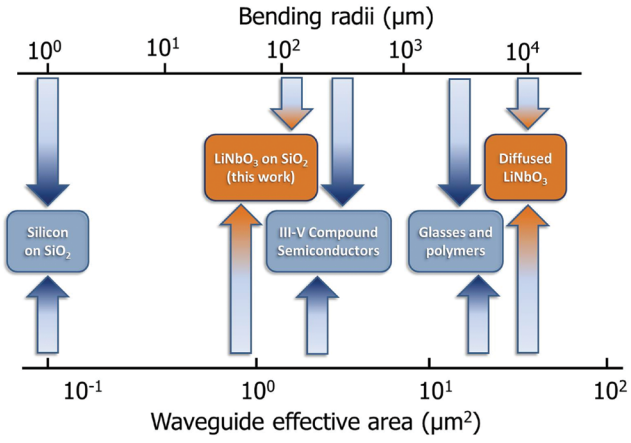

Figure 9 Improvements attained in $LiNbO_3$ waveguide platform in terms of waveguide effective areas and minimum radii for negligible (<~0.1 dB) bending loss at 90° turns based on the approach presented in the text and its comparison with other platforms. Δn denotes the approximate core-cladding index contrasts of the waveguide platforms [151].

advancement in the field of mid-IR photonics, a goal that can be achieved by silicon photonics.

Mid-IR silicon photonics has potential applications in the host of applications mentioned above, as well as lab-on-a-chip biochemical sensing for trace-gas detection and bio-agent sensing for environmental and homeland security monitoring, as well as industrial process control. It can also have several nonlinear-optical applications [185, 186]. The first demonstration of mid-IR Raman amplifiers [187, 188] suggested that nonlinear silicon photonic devices can be achieved. Indeed, TPA vanishes in the mid-IR regime (above ~2.2 μm to be more precise) and three-photon absorption are negligible at very high intensities [189]. Thus, the discussed omnipresent problem of nonlinear silicon devices in the near-IR, i.e., TPA-induced FCA, is inherently nonexistent in the mid-IR. Analytic and numerical works conducted at CREOL suggest that high-performance 3–5 μm nonlinear silicon photonic devices can be attained provided that low-loss waveguides and sources with high beam-quality are available [133, 190].

However, the standard SOI platform is generally not ideal for mid-IR photonics because the bottom cladding material, SiO_2, is very lossy over 2.5–2.9 μm and above 3.5 μm wavelengths [191]. Replacing SiO_2 with sapphire (transparent up to 4.3 μm), SiN (transparent up to 6.6 μm) or air (suspended silicon membrane, transparent up to 6.9 μm) as the bottom waveguide cladding layer, as well as Ge waveguides directly on Si (Ge-on-Si transparent up to 6.9 μm), were first proposed by Soref et al. [191]. All of these waveguide platforms have been demonstrated by other researchers, as reviewed below.

Available silicon-on-sapphire (SOS) wafers, originally developed for microelectronic applications, led to the demonstration of first Si-based mid-IR waveguides [192–194]. Low-loss waveguides and grating couplers on SOS were later demonstrated [195]. The author's group has also fabricated SOS waveguides (see Figure 10A). However, we have not been able to achieve low propagation loss (~12 dB/cm at 1.55 μm). The reason for this is not clear, but private communications with some other researchers, who have been using available SOS wafers in the market, suggest that quality variation of the Si thin layer grown epitaxially on sapphire substrates can cause this. Indeed, there has been some report on inherent twining defects in SOS [196]. At any rate and as mentioned, sapphire is transparent only up to 4.3 μm and silicon-on-nitride (SON) (see Figure 10B), air-clad all-silicon waveguides (see Figure 10C) and Ge-on-Si offer wider transparency ranges.

Ge-on-Si were first reported by Chang et al. [197]. Reduced-pressure chemical vapor deposition was employed to grow a 2-μm thick monocrystalline Ge relaxed layer on a Si and ~3-μm-wide stripes were fabricated by photolithography. These waveguides are inherently large due to the not very high index contrast between Ge and Si (~4 vs. 3.4) but for the same reason have relatively low propagation loss of ~3.6 dB/cm at 5.8 μm wavelength. More recently, Ge-on-Si thermo-optic phase shifters have been reported [198].

The author's group has demonstrated SON and all-silicon waveguides for the first time [199, 200]. We have also proposed and demonstrated the silicon on lithium niobate (SiLN) waveguide and modulator platform (see Figure 10D) [201, 202]. These three platforms are reviewed in detail in the following.

In principle, the discussed ion implantation and wafer slicing steps used for $LiNbO_3$-on-Si wafers can be employed to achieve SON wafers. But with the availability of SOI wafers, perhaps there is no need to repeat those steps in order to attain Si thin films. Rather, back-side etching of the Si substrate and the BOX layer can expose the thin Si layer. Accordingly, Figure 11 shows the processing steps for achieving SON dies [199]. Briefly, SOI handling dies are coated with low-stress PECVD SiN. Both CMP [203, 204] and spin-on-glass (SOG) [205, 206] techniques can in principle be used to achieve direct bonding. SOG was preferred due to its lower cost and ease of fabrication. Hydrophilic SiO_2 layers were deposited on both dies before bonding for improved adhesion. Initial room-temperature bonding at atmospheric pressure was followed by 60 min of annealing at 450°C. Then, the silicon handling wafer and the BOX layer are removed, resulting in a Si thin film residing on a SiN cladding layer on a Si substrate. Standard

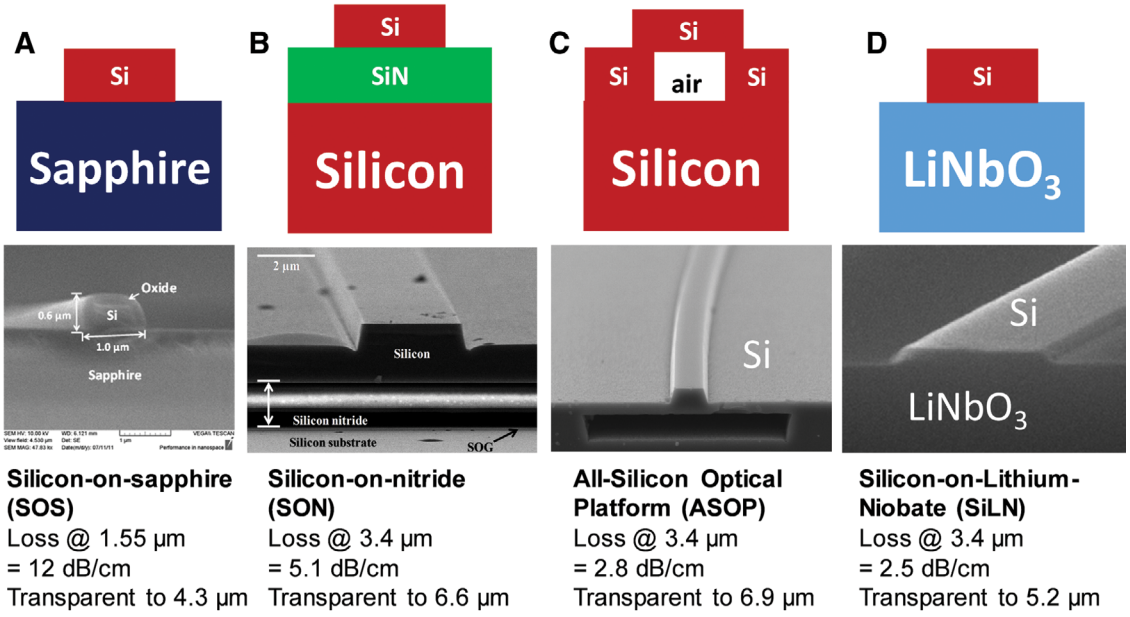

Figure 10 Four different mid-infrared waveguide technologies pursued at CREOL, their schematics and their measured propagation losses: (A) silicon-on-sapphire (SOS) (unpublished); (B) silicon-on-nitride (SON) [199]; (C) all-silicon optical platform (ASOP) [200]; (D) silicon-on-lithium-niobate (SiLN) [201, 202].

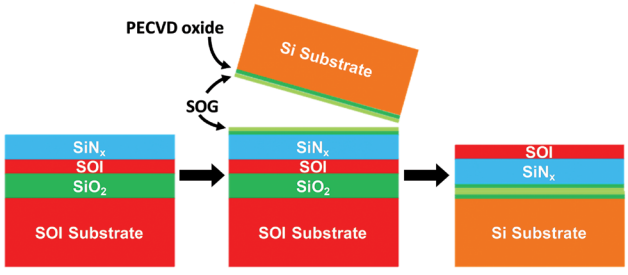

Figure 11 Fabrication steps of SON dies [199].

techniques were then used to fabricate ridge waveguides (see Figure 10B). At 3.39 µm wavelength, the propagation loss of the characterized waveguides is 5.1 dB/cm for the TM mode.

The next Si-based platform discussed in this review paper is perhaps not heterogeneous *per se* but indeed an all-silicon optical platform (ASOP) [200], i.e., air-clad suspended membrane waveguides. Nonetheless, since the processing steps for this truly homogeneous platform are based on bonding techniques discussed throughout this paper and it can be applied to enjoy the largest transparency range of ~2.5 octaves offered by silicon (1.2–6.9 µm), it is discussed here for completeness.

Suspended membrane waveguides for mid-IR were first demonstrated by local removal of BOX in SOI waveguides via forming an array of periodical holes in the top silicon layer adjacent to the rib waveguides [207]. However, due to the via forming and isotropic wet etching steps, the attained membranes become too wide to be mechanically and thermally stable, i.e., they are prone to vibrations, bowing and low thermal dissipation. The processing steps for the approach developed at CREOL, shown in Figure 12, address these shortcomings. An inverted SOI wafer is fusion-bonded to a bulk silicon substrate pre-patterned with trenches. Similar to the discussed SON processing steps, the SOI substrate and BOX are subsequently removed and a thin Si film on the buried trench is exposed. The air-filled trench acts as the bottom

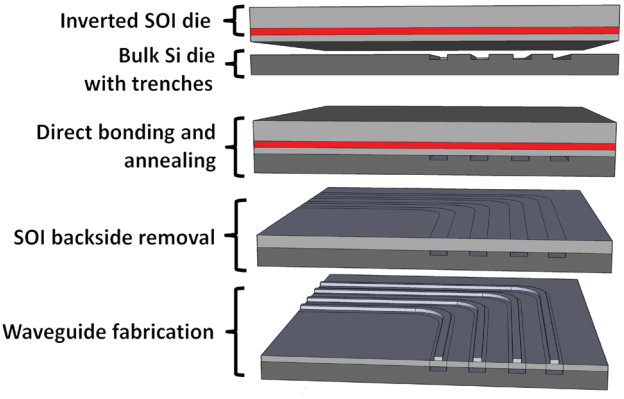

Figure 12 Fabrication steps of ASOP dies [200].

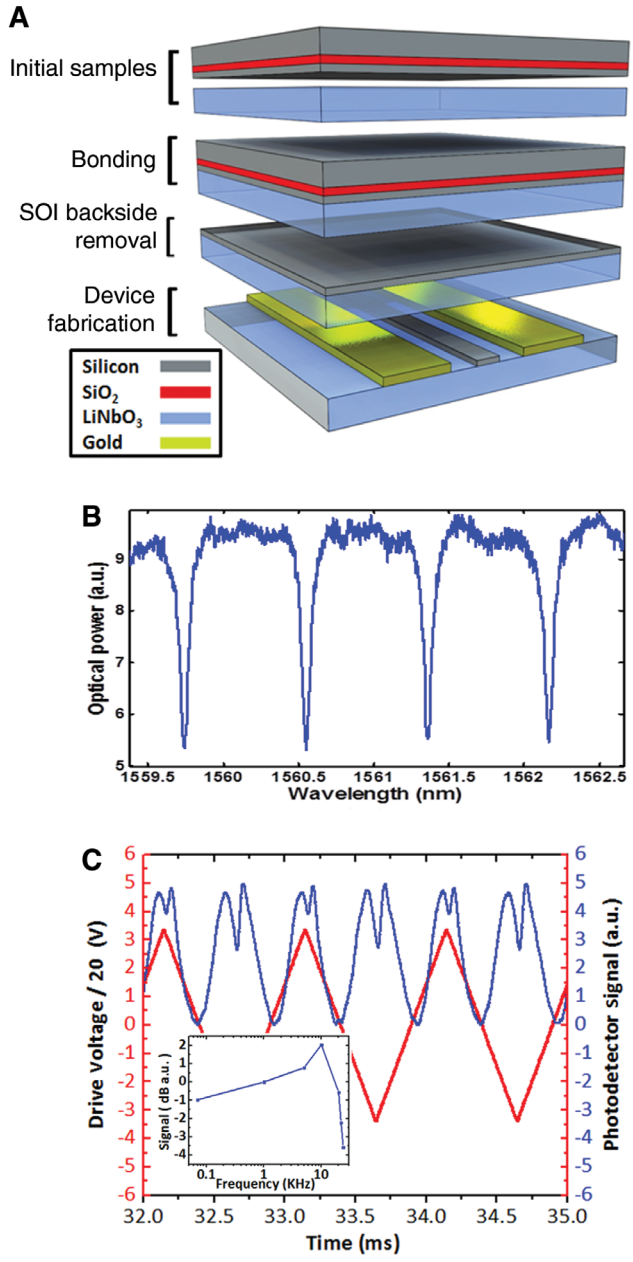

Figure 13 (A) Processing steps for SiLN wafers and devices [202]; (B) Measured spectral response of the SiLN microring resonators in the 1.55 μm range [201]; (C) Mid-IR SiLN modulator response at 3.39 μm wavelength. The red line is the modulator drive voltage divided by a factor of 20, and the blue line is the optical signal transmitted through the modulator, shifted for visibility. The inset shows the frequency response, limited by the detector speed [202].

waveguide cladding when waveguide ridges are formed by standard lithographic techniques. An SEM of the device is shown in Figure 10C. The waveguides have a TM-mode low propagation loss of 2.8 dB/cm at 3.39 μm. This is the first demonstration of a homogeneous all-silicon optical platform (ASOP). The first generation devices have a 16-μm-wide trenches and the membranes are mechanically very stable [200]. In an unpublished second generation of the devices, the width has been reduced to 12 μm. The depth of the trench can be freely controlled and the formed fusion-sealed internal channel can be potentially used for microfluidic or gas-sensing applications.

The last mid-IR platform discussed in this review paper is based on bonding a Si thin film on a $LiNbO_3$ substrate. The motivation for developing this silicon-on-lithium-niobate or SiLN platform at CREOL is primarily to achieve EO modulator in the mid-IR range. Microring resonators and grating couplers characterized at 1.55 μm [201] and EO MZI modulators at 3.4 μm [202] have been demonstrated. As shown in Figure 13A, room-temperature plasma-assisted bonding was employed to directly bond an SOI die with a $LiNbO_3$ die. Then, the dies are annealed at low temperature. Wet etching of the SOI backside, exposes a 220 nm-thick crystalline silicon layer on $LiNbO_3$. The relatively large index contrast of Si versus $LiNbO_3$ (~3.4 vs. ~2.1) provides an opportunity to achieve compact oxide-less channel (0.6-μm wide in Figure 10D) Si waveguide directly on an EO-active substrate. Microring resonators were demonstrated at near-IR wavelengths. Their propagation loss is as low as 3.0 dB/cm for the TM mode at 1.55 μm (see Figure 13B) with a ring radius of 130 μm [201]. According to mode simulations and at 3.4 μm wavelength, ~24% of the optical mode resides in $LiNbO_3$. Hence, relatively strong EO modulators can be envisaged, as we have very recently demonstrated (see Figure 13C) [202]. This is the first demonstration of a mid-IR EO modulator. The devices attain a modulation depth of 8 dB, a $V_\pi.L$ of 26 V.cm at low frequencies, a propagation loss of 2.5 dB/cm, and an insertion loss of ~3 dB, all characterized at a wavelength of 3.4 μm.

8 Concluding remarks

Herbert Spencer, the famous nineteenth century English polymath once wrote: “From the remotest past which Science can fathom, up to the novelties of yesterday, that in which Progress essentially consists, is the transformation of the homogeneous to the heterogeneous” [208]. Such a transformation appears to be the destiny of progress in the science and technology of electronic-photonic integrated circuits. It may be unwise to make predictions for any field of science and engineering, but based on the review of the field in this paper, the following remarks are cautiously made. It appears that in the foreseeable future, heterogeneous technologies, that combine group

IV and III–V semiconductors, and perhaps $LiNbO_3$ and other materials such as nitride semiconductors and high-index dielectrics, will most likely dominate integrated optoelectronics. Electronics will most likely be based on Si CMOS and lasers will most likely be on III–Vs. Prevailing materials and device platforms for other functionalities are much more debatable and predicting them is more difficult, hence less assertive adjectives are chosen in the following. Photodetectors will likely be on Ge, but perhaps on III–Vs. Modulators could be based either on free-carrier-plasma effect in Si, EO or EA effect in III–Vs or EA in GeSi, or EO in $LiNbO_3$. Passive devices (waveguides, filters, etc.) will likely be on Si due to its inexpensiveness and low loss.

Acknowledgments: The author would like to thank the past and present members of his research group, J. Chiles, S. Khan, J. Ma, P. Rabiei and A. Rao, for their contributions to some of the works reviewed here. The author would also thank J. Chiles and A. Rao for critically reading the manuscript. The works are being supported by the United States' Office of Naval Research (ONR) Young Investigator Program (YIP) under the Grant Number 11296285 and the National Science Foundation CAREER Program under Award Number ECCS-1150672.

References

[1] Hall RN, Fenner GE, Kingsley JD, Soltys TJ, Carlson RO. Coherent light emission from GaAs Junctions. Phys Rev Lett 1962;9:366–9.
[2] Alferov ZI, Kazarinov RF. Semiconductor laser with electric pumping. Inventor's Certificate 181737 [in Russian], Appli. 950840, priority as of March 30, 1963.
[3] Kroemer H. Semiconductor laser with electric pumping. U.S. Patent 3 309 553, Filed Aug. 16, 1963.
[4] Dupuis RD, Dapkus PD. Room temperature operation of $Ga_{1-x}Al_xAs$/GaAs double-heterostructure lasers grown by metalloorganic chemical vapor deposition. Appl Phys Lett 1977;31:466–8.
[5] Dupuis RD, Dapkus PD, Holonyak N, Rezek EA, Chin R. Room temperature operation of quantum-well $Ga_{1-x}Al_xAs$-GaAs laser diodes grown by metalorganic chemical vapor deposition. Appl Phys Lett 1978;32:295–7.
[6] Soref RA, Lorenzo JP. Single-crystal silicon – A new material for 1.3 and 1.6 μm integrated-optical components. Elec Lett 1985;21:953–4.
[7] Soref RA, Lorenzo JP. All-silicon active and passive guided-wave components for $\lambda = 1.3$ and 1.6 μm. IEEE J Quantum Elect 1986;22:873–9.
[8] Soref RA, Bennett BR. Electrooptical effects in silicon. IEEE J Quantum Elect 1987;23:123–9.
[9] Lorenzo JP, Soref RA. 1.3 μm electro-optic silicon switch. Appl Phys Lett 1987;51:6–8.
[10] Soref RA. Silicon-based optoelectronics. Proc IEEE 1993;81:1687–706.
[11] Jalali B, Yegnanarayanan S, Yoon T, Yoshimoto T, Rendina I, Coppinger F. Advances in silicon-on-insulator optoelectronics. IEEE J Sel Top Quant Electron 1998;4:938–47.
[12] Lipson M. Guiding, modulating, and emitting light on silicon – challenges and opportunities. J Lightwave Technol 2005;23:4222–38.
[13] Jalali B, Fathpour S. Silicon photonics. J Lightwave Technol 2006;24:4600–15.
[14] Soref RA. The past, present, and future of silicon photonics. IEEE J Sel Top Quant Electron 2006;12:1678–87.
[15] Jalali B. Can silicon change photonics? Phys Status Solidi A 2008;205:213–24.
[16] Pavesi L, Lockwood DJ, eds., Silicon photonics. Heidelberg-Berlin, Germany, Springer Verlag, 2004.
[17] Reed GT, Knights AP. Silicon photonics: an introduction. West Sussex, UK, John Wiley & Sons, 2004.
[18] Reed GT, ed. Silicon photonics: the state of the art. West Sussex, England, John Wiley & Sons, 2008.
[19] Khriachtchev L, ed. Silicon nanophotonics. Singapore, World Scientific Publishing, 2009.
[20] Fathpour S, Jalali B, eds. Silicon photonics for telecommunications and biomedicine. Boca Raton, FL, CRC Press, 2012.
[21] Soref RA, Schmidtchen J, Petermann K. Large single-mode rib waveguides in GeSi and Si-on-SiO_2. IEEE J Quant Electron 1991;27:1971–4.
[22] Schmidtchen J, Splett A, Schuppert B, Petermann K, Burbach G. Low-loss single mode optical waveguides with large cross-section in silicon-on-insulator. Electron Lett 1991;27:1486–7.
[23] Rickman AG, Reed GT, Namavar F. Silicon-on-insulator optical rib waveguide loss and mode characteristics. J Lightwave Technol 1994;12:1771–6.
[24] Zhao CZ, Li GZ, Liu EK, Gao Y, Liu XD. Silicon on insulator Mach-Zehnder waveguide interferometers operating at 1.3 μm. Appl Phys Lett 1995;67:2448–9.
[25] Trinh PD, Yegnanarayanan S, Jalali B. Integrated optical directional couplers in silicon-on-insulator. Electron Lett 1995;31:2097.
[26] Trinh PD, Yegnanarayanan S, Jalali B. 5×9 integrated optical star coupler in silicon-on-insulator technology. IEEE Photon Technol Lett 1996;8:794–6.
[27] Pezeshki B, Agahi F, Kash JA, Welser JJ, Wang WK. Wavelength-selective waveguide photodetectors in silicon-on-insulator. Appl Phys Lett 1996;68:741–3.
[28] Izumi K, Doken M, Ariyoshi H. C.M.O.S. devices fabricated on buried SiO_2 layers formed by oxygen implantation into silicon. Electron Lett 1978;14:593–4.
[29] Lasky JB, Stiffler SR, White FR, Abernathy JR. Silicon-on-insulator (SOI) by bonding and etch-back. Proc IEEE Int Electron Dev Meeting 1985;31:684–7.
[30] Bruel M. A new silicon-on-insulator material technology. Electron Lett 1995;31:1201–2.
[31] Celler GK, Cristoloveanu S. Frontiers of silicon-on-insulator. J Appl Phys 2003;93:4955–78.

[32] Jalali B, Dimitropoulos D, Raghunathan V, Fathpour S. Silicon lasers. In: Reed G.T., ed. Silicon photonics: State of the Art. West Sussex, England, John Wiley & Sons, 2008.
[33] Gunn C. CMOS photonics for high-speed interconnects. IEEE Micro 2006;26:58–66.
[34] Liang TK, Tsang HK. Role of free carriers from two-photon absorption in Raman amplification in silicon-on-insulator waveguides. Appl Phys Lett 2004;84:2745–7.
[35] Claps R, Raghunathan V, Dimitropoulos D, Jalali B. Influence of nonlinear absorption on Raman amplification in silicon waveguides. Opt Express 2004;12:2774–80.
[36] Luryi S, Kastalsky A, Bean JC. New infrared detector on a silicon chip. IEEE Trans Electron Dev 1984;31:1135–9.
[37] Temkin H, Bean JC, Pearsall TP, Olsson NA, Lang DV. High photoconductive gain in Ge_xSi_{1-x}/Si strained-layer superlattice detectors operating at 1.3 μm. Appl Phys Lett 1986;49:155–7.
[38] Jalali B, Levi AFJ, Ross F, Fitzgerald EA. SiGe waveguide photodetectors grown by rapid thermal chemical vapour deposition. Electron Lett 1992;28:269–71.
[39] Jalali B, Naval L, Levi AFJ. Si-based receivers for optical data links. J Lightwave Technol 1994;12:930–5.
[40] Samavedam SB, Currie MT, Langdo TA, Fitzgerald EA. High-quality germanium photodiodes integrated on silicon substrates using optimized relaxed graded buffers. Appl Phys Lett 1998;73:2125–7.
[41] Colace L, Masini G, Assanto G. Ge-on-Si approaches to the detection of near-infrared light. IEEE J Quant Electron 1999;35:1843–52.
[42] Jutzi M, Berroth M, Wohl G, Oehme M, Kasper E. Ge-on-Si vertical incidence photodiodes with 39-GHz bandwidth. IEEE Photon Technol Lett 2005;17:1510–2.
[43] Schow CL, Schares L, Koester SJ, Dehlinger G, John R, Doany FE. A 15-Gb/s 2.4-V optical receiver using a Ge-on-SOI photodiode and a CMOS IC. IEEE Photon Technol Lett 2006;18:1981–3.
[44] Yin T, Cohen R, Morse MM, Sarid G, Chetrit Y, Rubin D, Paniccia MJ. 31 GHz Ge n-i-p waveguide photodetectors on silicon-on-insulator substrate. Opt Express 2007;15:13965–71.
[45] Vivien L, Osmond J, Fédéli JM, Marris-Morini D, Crozat P, Damlencourt JF, Cassan E, Lecunff Y, Laval S. 42 GHz p.i.n Germanium photodetector integrated in a silicon-on-insulator waveguide. Opt Express 2009;17:6252–7.
[46] Park S, Tsuchizawa T, Watanabe T, Shinojima H, Nishi H, Yamada K, Ishikawa Y, Wada K, Itabashi S. Monolithic integration and synchronous operation of germanium photodetectors and silicon variable optical attenuators. Opt Express 2010;18:8412–21.
[47] Michel J, Liu J, Kimerling LC. High-performance Ge-on-Si photodetectors. Nat Photonics 2010;4:527–34.
[48] Liao S, Feng NN, Feng D, Dong P, Shafiiha R, Kung CC, Liang H, Qian W, Liu Y, Fong J, Cunningham JE, Luo Y, Asghari M. 36 GHz submicron silicon waveguide germanium photodetector. Opt Express 2011;19:10967–72.
[49] Tsuchizawa T, Yamada K, Watanabe T, Park S, Nishi H, Rai K, Shinojima H, Itabashi SI. Monolithic integration of silicon-, germanium-, and silica-based optical devices for telecommunications applications. IEEE J Select Top Quant Electron 2011;17:516–25.
[50] Chen L, Doerr CR, Buhl L, Baeyens Y, Aroca RA. Monolithically integrated 40-wavelength demultiplexer and photodetector array on silicon. IEEE Photonics Technol Lett 2011;23:869–71.
[51] DeRose CT, Douglas C, Trotter DC, Zortman WA, Starbuck AL, Fisher M, Watts MR, Davids PS. Ultra compact 45 GHz CMOS compatible Germanium waveguide photodiode with low dark current. Opt Express 2011;19:24897–904.
[52] Camacho-Aguilera RE, Cai Y, Patel N, Bessette JT, Romagnoli M, Kimerling LC, Jurgen Michel. An electrically pumped germanium laser. Opt Express 2012;20:11316–20.
[53] Kasper E, Kittler M, Oehme M, Arguirov T. Germanium tin: silicon photonics toward the mid-infrared. Photon Research 2013;1:69–76.
[54] Terui H, Yamada Y, Kawachi M, Kobayashi M. Hybrid integration of a laser diode and high-silica multimode optical channel waveguide on silicon. Electron Lett 1985;21:646–8.
[55] Joppe JL, de Krijger AJT, Noordman OFJ. Hybrid integration of laser diode and monomode high contrast slab waveguide on silicon. Electron Lett 1991;27:162–3.
[56] Friedrich EL, Oberg MG, Broberg B, Nilsson S, Valette S. Hybrid integration of semiconductor lasers with Si-based single-mode ridge waveguides. J Lightwave Technol 1992;10:336–40.
[57] Sasaki J, Itoh M, Tamanuki T, Hatakeyama H, Kitamura S, Shimoda T, Kato T. Multiple-chip precise self-aligned assembly for hybrid integrated optical modules using Au-Sn solder bumps. IEEE Trans Adv Packaging 2001;24:569–75.
[58] Huang A, Gunn C, Li GL, Liang Y, Mirsaidi S, Narasimha A, Pinguet, T. A 10 Gb/s photonic modulator and WDM MUX/DEMUX integrated with electronics in 0.13 μm SOI CMOS. 2006 IEEE International Solid-State Circuits Conference, Digest of Technical Papers, 922–929, San Francisco, CA, 2006.
[59] Chu T, Fujioka N, Ishizaka M. Compact, lower-power-consumption wavelength tunable laser fabricated with silicon photonic-wire waveguide micro-ring resonators. Opt Express 2009;17:14063–8.
[60] Ohira K, Kobayashi K, Iizuka N, Yoshida H, Ezaki M, Uemura H, Kojima A, Nakamura K, Furuyama H, Shibata H. On-chip optical interconnection by using integrated III-V laser diode and photodetector with silicon waveguide. Opt Express 2010;18:15440–7.
[61] Tanaka S, Jeong SH, Sekiguchi S, Kurahashi T, Tanaka Y, Morito K. High-output-power, single-wavelength silicon hybrid laser using precise flip-chip bonding technology. Opt Express 2012;20:28057–69.
[62] Chen HZ, Palaski J, Yariv A, Morkoc H. High-frequency modulation of AlGaAs/GaAs lasers grown on Si substrate by molecular beam epitaxy. Appl Phys Lett 1988;52:605–7.
[63] Anderson RL. Experiments on Ge-GaAs heterojunctions. Solid State Electron 1962;5:341–4.
[64] Aspnes DE, Stunda AA. Chemical etching and cleaning procedures for Si, Ge, and some III-V compound semiconductors. Appl Phys Lett 1981;39:316–8.
[65] Fischer R, Masselink WT, Klem J, Henderson T, McGlinn TC, Klein MV, Morkoc H, Mazur JH, Washburn J. Growth and properties of GaAs/AlGaAs on nonpolar substrates using molecular beam epitaxy. J Appl Phys 1985;58:374–81.
[66] Petroff PM. Nucleation and growth of GaAs on Ge and the structure of antiphase boundaries. J Vac Sci Tech B 1986;4:874–7.
[67] Reddy UK, Houdre R, Munns G, Ji G, Morko H, Longerbone M, Davis L, Gu BP, Otuska N. Investigation of GaAs/(Al,Ga)As multiple quantum wells grown on Ge and Si substrates by molecular-beam epitaxy. J Appl Phys 1987;62:4858–62.
[68] Groenert ME, Leitz CW, Pitera AJ, Yang V, Lee H, Ram RJ, Fitzgerald EA. Monolithic integration of room-temperature cw GaAs/

AlGaAs lasers on Si substrates via relaxed graded GeSi buffer layers. J Appl Phys 2003;93:362–7.
[69] Sakai S, Soga T, Takeyasu M, Umeno M. Room-temperature laser operation of AlGaAs-GaAs double heterostructures fabricated on Si substrates by metalorganic chemical vapor-deposition. Appl Phys Lett 1986;48:413–4.
[70] Fischer R, Kopp W, Morkoc H, Pion M, Specht A, Burkhart G, Appelman H, McGougan D, Rice R. Low threshold laser operation at room-temperature in GaAs/(Al,Ga)As structures grown directly on (100) Si. Appl Phys Lett 1986;48:1360–1.
[71] Yang J, Mi Z, Bhattacharya P. Grooved-coupled InGaAs/GaAs quantum dot laser/waveguide on silicon. J Lightwave Technol 2007;25:1826–31.
[72] Yang J, Bhattacharya P. Integration of epitaxially-grown InGaAs/GaAs quantum dot lasers with hydrogenated amorphous silicon waveguides on silicon. Opt Express 2008;16:5136–40.
[73] Heck MJR, Bauters J, Davenport M, Doylend JK, Jain S, Kurczveil G, Srinivasan S, Tang Y, Bowers JE. Hybrid silicon photonic integrated circuit technology. IEEE J Sel Topics Quant Electron 2013;19:6100117.
[74] Keyvaninia S, Roelkens G, Van Thourhout D, Jany C, Lamponi M, Le Liepvre A, Lelarge F, Make D, Duan GH, Bordel D, Fedeli JM. Demonstration of a heterogeneously integrated III-V/SOI single wavelength tunable laser. Opt Express 2013;21:3784–92.
[75] Creazzo T, Marchena E, Krasulick SB, Yu PK, Van Orden D, Spann JY, Blivin CC, He L, Cai H, Dallesasse JM, Stone RJ, Mizrahi A. Integrated tunable CMOS laser. Opt Express 2013;21:28048–53.
[76] Crumbaker TE, Lee HY, Hafich MJ, Robinson GY. Growth on InP on Si substrates by molecular beam epitaxy. Appl Phys Lett 1989;54:140–2.
[77] Sugo M, Takanashi Y, Al-Jassim MM, Yamaguchi M. Heteroepitaxial growth and characterization of InP on Si substrates. J Appl Phys 1990;68:540–7.
[78] Wuu DS, Horng RH, Lee MK. Indium phosphide on silicon heteroepitaxy: lattice deformation and strain relaxation. J Appl Phys 1990;68:3338–42.
[79] Itakura H, Suzuki T, Jiang ZK, Soga T, Jimbo T, Umeno M. Effect of InGaAs/InP strained layer superlattice in InP-on-Si. J Cryst Growth 1991;115:154–7.
[80] Cerutti L, Rodriguez JB, Tournie E. GaSb-based laser, monolithically grown on silicon substrate, emitting at 1.55 μm at room temperature. IEEE Photon Tech Lett 2010;22:553–5.
[81] Roelkens G, Van Thourhout D, Baets R, Nötzel R, Smit M. Laser emission and photodetection in an InP/InGaAsP layer integrated on and coupled to a silicon-on-insulator waveguide circuit. Opt Express 2006;14:8154–9.
[82] Rayleigh L. A study of glass surfaces in optical contact. Proc Phys Soc 1936;A156:326–49.
[83] Shimbo M, Furukawa K, Fukuda K, Tanzawa K. Silicon-to-silicon direct bonding method. J Appl Phys 1986;60:2987–9.
[84] Seassal C, Rojo-Romeo P, Letartre X, Viktorovitch P, Hollinger G, Jalaguier E, Pocas S, Aspar B. InP microdisk lasers on silicon wafers: CW room temperature operation at 1.6 μm. Electron Lett 2001;37:222–3.
[85] Rojo RP, Van Campenhout J, Regreny P, Kazmierczak A, Seassal C, Letartre X, Hollinger G, Van Thourhout D, Baets R, Fedeli JM, Di Cioccio L. Heterogeneous integration of electrically driven microdisk based laser sources for optical interconnects and photonic ICs. Opt Express 2006;14:3864–71.
[86] Pasquariello D, Hjort K. Plasma-assisted InP-to-Si low temperature wafer bonding. IEEE J Sel Top Quant Electron 2002;8:118–31.
[87] Seung CJ, Djordjev K, Choi SJ, Dapkus PD. Microdisk lasers vertically coupled to output waveguides. IEEE Photon Technol Lett 2003;15:1330–2.
[88] Hattori HT, Seassal C, Touraille E, Rojo-Romeo P, Letartre X, Hollinger G, Viktorovitch P, Di Cioccio L, Zussy M, Melhaoui LE, Fedeli JM. Heterogeneous integration of microdisk lasers on silicon strip waveguides for optical interconnects. IEEE Photon Technol Lett 2006;18:223–5.
[89] Pasquariello D, Lindeberg M, Hedlund C, Hjort K. Surface energy as a function of self-bias voltage in oxygen plasma wafer bonding. Sensor Actuator 2000;82:239–44.
[90] Pasquariello D, Hedlund C, Hjort K. Oxidation and induced damages in oxygen plasma in situ wafer bonding. J Electrochem Soc 2000;147:2699–702.
[91] Pasquariello D, Camacho M, Hjort K, Dozsa L, Szentpali B. Evaluation of InP to Si heterobonding. Mater Sci Eng B 2001;B80:134–7.
[92] Park H, Fang AW, Kodama S, Bowers JE. Hybrid silicon evanescent laser fabricated with a silicon waveguide and III-V offset quantum wells. Opt Express 2005;13:9460–4.
[93] Fang AW, Park H, Cohen O, Jones R, Paniccia MJ, Bowers JE. Electrically pumped hybrid AlGaInAs-silicon evanescent laser. Opt Express 2006;14:9203–10.
[94] Liang D, Bowers JE.Recent progress in lasers on silicon. Nat Photonics 2010;4:511–7.
[95] Sun X, Zadok A, Shearn MJ, Diest KA, Ghaffari A, Atwater HA, Scherer A, Yariv A. Electrically pumped hybrid evanescent Si/InGaAsP lasers. Opt Lett 2009;34:1345–7.
[96] Van Campenhout J, Romero PR, Regreny P, Seassal C, Van Thourhout D, Verstuyft S, Di Cioccio L, Fedeli JM, Lagahe C, Baets R. Electrically pumped InP-based microdisk lasers integrated with a nanophotonic silicon-on-insulator waveguide circuit. Opt Express 2007;15:6744–9.
[97] Keyvaninia S, Verstuyft S, Van Landschoot L, Lelarge F, Duan G-H, Messaoudene S, Fedeli JM, De Vries T, Smalbrugge B, Geluk EJ, Bolk J, Smit M, Morthier G, Van Thourhout D, Roelkens G. Heterogeneously integrated III-V/silicon distributed feedback lasers. Opt Lett 2013;38:5434–7.
[98] Claps R, Dimitropoulos D, Han Y, Jalali B. Observation of Raman emission in silicon waveguides at 1.54 μm. Opt Express 2002;10:1305–13.
[99] Claps R, Dimitropoulos D, Raghunathan V, Han Y, Jalali B. Observation of stimulated Raman scattering in silicon waveguides. Opt Express 2003;11:1731–9.
[100] Claps R, Raghunathan V, Dimitropoulos D, Jalali B. Anti-stokes Raman conversion in silicon waveguides. Opt Express 2003;11:2862–72.
[101] Boyraz O, Jalali B. Demonstration of a silicon Raman laser. Opt Express 2004;12:5269–73.
[102] Raghunathan V, Claps R, Dimitropoulos D, Jalali B. Wavelength conversion in silicon using Raman induced four-wave mixing. Appl Phys Lett 2004;85:34–6.
[103] Raghunathan V, Claps R, Dimitropoulos D, Jalali B. Parametric Raman wavelength conversion in scaled silicon waveguides. J Lightwave Technol 2005;23:2094–102.

[104] Boyraz O, Indukuri T, Jalali B. Self-phase modulation-induced spectral broadening in silicon waveguides. Opt Express 2004;12:829–34.
[105] Boyraz O, Koonath P, Raghunathan V, Jalali B. All optical switching and continuum generation in silicon waveguides. Opt Express 2004;12:4094–102.
[106] Leuthold J, Koos C, Freude W. Nonlinear silicon photonics. Nat Photonics 2010;4:535–44.
[107] Rong H, Jones R, Liu A, Cohen O, Hak D, Fang A, Paniccia M. A continuous-wave Raman silicon laser. Nature 2005;433:725–8.
[108] Fathpour S, Tsia KK, Jalali B. Energy harvesting in silicon Raman amplifiers. Appl Phys Lett 2006;89:061109.
[109] Fathpour S, Jalali B. Energy harvesting in silicon optical modulators. Opt Express 2006;14:10795–9.
[110] Tsia KK, Fathpour S, Jalali B. Energy harvesting in silicon wavelength converter. Opt Express 2006;14:12327–33.
[111] Fathpour S, Tsia KK, Jalali B. Two-photon photovoltaic effect in silicon. IEEE J Quantum Electron 2007;43:1211–7.
[112] Jalali B, Fathpour S, Tsia KK. Green silicon photonics. Opt Photonics News 2009;20:18–23.
[113] Dimitropoulos D, Fathpour S, Jalali B. Intensity dependence of the carrier lifetime in silicon Raman lasers and amplifiers. Appl Phys Lett 2005;87:261108.
[114] Krause M, Renner H, Fathpour S, Jalali B, Brinkmeyer E. Raman-gain enhancement in cladding-pumped silicon waveguides. IEEE J Quantum Electron 2008;44:692–704.
[115] Liu Y, Tsang HK. Nonlinear absorption and Raman gain in helium-ion-implanted silicon waveguides. Opt Lett 2006;31:1714–6.
[116] Narayanan K, Preble SF. Optical nonlinearities in hydrogenated-amorphous silicon waveguides. Opt Express 2010;18:8998–9005.
[117] Kuyken B, Ji H, Clemmen S. Nonlinear properties of and nonlinear processing in hydrogenated amorphous silicon waveguides. Opt Express 2011;19:146–53.
[118] Grillet C, Carletti L, Monat C. Amorphous silicon nanowires combining high nonlinearity, FOM and optical stability. Opt Express 2012;20:22609–15.
[119] Ikeda K, Saperstein RE, Alic N, Fainman Y. Thermal and Kerr nonlinear properties of plasma-deposited silicon nitride/silicon dioxide waveguides. Opt Express 2008;16:12987–94.
[120] Tan DTH, Ikeda K, Sun PC, Fainman Y. Group velocity dispersion and self phase modulation in silicon nitride waveguides. Appl Phys Lett 2010;96:061101.
[121] Moss DJ, Morandotti R, Gaeta AL, Lipson M. New CMOS-compatible platforms based on silicon nitride and Hydex for nonlinear optics. Nat Photonics 2013;7:597–607.
[122] Duchesne D, Ferrera M, Razzari L. High performance, low-loss nonlinear integrated glass waveguides. PIERS Online 2010;6:283–6.
[123] Razzari L, Duchesne D, Ferrera M. CMOS-compatible integrated optical hyper-parametric oscillator. Nat Photonics 2010;4:41–5.
[124] Madden SJ, Choi DY, Bulla DA, Rode AV, Luther-Davies B, Ta'eed VG, Pelusi MD, Eggleton BJ. Long, low loss etched As_2S_3 chalcogenide waveguides for all-optical signal regeneration. Opt Express 2007;15:14414–21.
[125] Gai X, Madden S, Choi DY, Bulla D, Luther-Davies B. Dispersion engineered $Ge_{11.5}As_{24}Se_{64.5}$ nanowires with a nonlinear parameter of 136000$W^{-1}km^{-1}$ at 1550 nm. Opt Express 2010;18:18866–74.
[126] Eggleton BJ, Luther-Davies B, Richardson K. Chalcogenide photonics. Nat Photonics 2011;5:141–8.
[127] Tai CY, Wilkinson JS, Perney NMB, Netti M, Cattaneo F, Finlayson C, Baumberg J. Determination of nonlinear refractive index in a Ta_2O_5 rib waveguide using self-phase modulation. Opt Express 2004;12:5110–6.
[128] Unal B, Tai CY, Shepherd DP, Wilkinson JS, Perney NMB, Netti MC, Parker GJ. Nd:Ta_2O_5 rib waveguide lasers. Appl Phys Lett 2005;86:021110.
[129] Mills JD, Chaipiboonwong T, Brocklesby WS, Charlton MD, Zoorob ME, Netti C, Baumberg JJ. Observation of the developing optical continuum along a nonlinear waveguide. Optics Lett 2006;31:2459–61.
[130] Chen RY, Charlton MD, Lagoudakis PG. Chi3 dispersion in planar tantalum pentoxide waveguides in the telecommunications window. Optics Lett 2009;34:1135–7.
[131] Rabiei P, Ma J, Khan S, Chiles J, Fathpour S. Submicron tantalum pentoxide optical waveguide and microring resonators fabricated by selective oxidation of refractory metal. Opt Express 2013;21:6967–72.
[132] Rabiei P, Rao A, Ma J, Khan S, Chiles J, Fathpour S. Low-loss and high index-contrast tantalum pentoxide microring resonators and grating couplers on silicon substrates. Opt Lett 2014;39:5379–83.
[133] Ma J, Fathpour S. Noise characteristics of mid- and near-infrared nonlinear silicon photonic devices. IEEE J Lightwave Technol 2013;31:3181–7.
[134] Jacobsen RS, Andersen KN, Borel PI, Fage-Pedersen J, Frandsen LH, Hansen O, Kristensen M, Lavrinenko AV, Moulin G, Ou H, Peucheret C, Zsigri B, Bjarklev A. Strained silicon as a new electro-optic material. Nature 2006;441:199–202.
[135] Chmielak B, Waldow M, Matheisen C, Ripperda C, Bolten J, Wahlbrink T, Nagel M, Merget F, Kurz H. Pockels effect based fully integrated, strained silicon electro-optic modulator. Opt Express 2011;19:17212–9.
[136] Cazzanelli M, Bianco F, Borga E. Second-harmonic generation in silicon waveguides strained by silicon nitride. Nat Mater 2012;11:148–54.
[137] Tsia KK, Fathpour S, Jalali B. Electrical control of parametric processes in silicon waveguides. Opt Express 2008;16:9838–43.
[138] Tsia KK, Fathpour S, Jalali B. Electrical tuning of birefringence in silicon waveguides. Appl Phys Lett 2008;92:061109.
[139] Reed GT, Mashanovich G, Gardes FY, Thomson DJ. Silicon optical modulators. Nat Photonics 2010;4:518.
[140] Thomson DJ, Gardes FY, Fedeli JM, Zlatanovic S, Hu Y, Kuo BPP, Myslivets E, Alic N, Radic S, Mashanovich GZ, Reed GT. 50-Gb/s silicon optical modulator. IEEE Photon Technol Lett 2012;24:234.
[141] Tu X, Liow TY, Song J, Luo X, Fang Q, Yu M, Lo G-Q. 50-Gb/s silicon optical modulator with traveling-wave electrodes. Opt Express 2013;21:12776–82.
[142] Wooten EL, Kissa KM, Yi-Yan A. A review of lithium niobate modulators for fiber-optic communications systems. IEEE J Select Topics Quant Electron 2000;6:69–72.
[143] Noguchi K, Mitomi O, Miyazawa H. Millimeter-wave Ti:$LiNbO_3$ optical modulators. IEEE J Lightwave Technol 1998;16:615–9.

[144] Xiong C, Pernice W, Ryu KK. Integrated GaN photonic circuits on silicon (100) for second harmonic generation. Opt Express 2011;19:10462–70.
[145] Pernice WHP, Xiong C, Schuck C, Tang HX. Second harmonic generation in phase matched aluminum nitride waveguides and micro-ring resonators. Appl Phys Lett 2012;100:223501.
[146] Leuthold J, Koos C, Freude W, Alloatti L, Palmer R, Korn D, Pfeifle J, Lauermann M, Dinu R, Wehrli S, Jazbinsek M, Gunter P, Waldow M, Wahlbrink T, Bolten J, Kurz H, Fournier M, Fedeli J-M, Yu H, Bogaerts W. Silicon-organic hybrid electro-optical devices. IEEE J Select Top Quant Electron 2013;19:3401413.
[147] Qasaimeh O, Bhattacharya P, Croke ET. SiGe-Si quantum-well electroabsorption modulators. IEEE Photon Technol Lett 1998;807–9.
[148] Kuo Y, Lee YK, Ge Y, Ren S, Roth JE, Kamins TI, Miller DAB, Harris JS. Strong quantum-confined Stark effect in germanium quantum-well structures on silicon. Nature 2005;437:1334–6.
[149] Liu JF, Beals M, Pomerene A. Waveguide-integrated, ultralow-energy GeSi electro-absorption modulators. Nat Photonics 2008;2:433–7.
[150] Feng D, Qian W, Liang H, Kung C-C, Zhou Z, Li Z, Levy JS, Shafiiha R, Fong J, Luff BJ, Asghari M. High-speed GeSi electro-absorption modulator on the SOI waveguide platform. IEEE J Sel Top Quantum Electron 2013;19:3401710.
[151] Rabiei P, Ma J, Khan S, Chiles J, Fathpour S. Heterogeneous lithium niobate photonics on silicon substrates. Opt Express 2013;23:25573–81.
[152] Wong K. Properties of lithium niobate. London, UK, INSPEC, 2002.
[153] Howerton MM, Moeller PR, Greenblatt AS, a Krähenbühl R. Fully packaged, broad-band LiNbO3 modulator with low drive voltage. IEEE Photon Technol Lett 2000;12:792–4.
[154] Chiba A, Sakamoto T, Kawanishi T, Higuma K, Sudo M, Ichikawa J. 16-level quadrature amplitude modulation by monolithic quad-parallel Mach-Zehnder optical modulator. Electron Lett 2010;46:220–2.
[155] Sakashita Y, Segawa H. Preparation and characterization of $LiNbO_3$ thin films produced by chemical-vapor deposition. J Appl Phys 1995;77:5995–9.
[156] Yoon JG, Kim K. Growth of highly textured $LiNbO_3$ thin film on Si with MgO buffer layer through the sol-gel process. Appl Phys Lett 1996;68:2523–5.
[157] Griffel G, Ruschin S, Croitoru N. Linear electro-optic effect in sputtered polycrystalline $LiNbO_3$ films. Appl Phys Lett 1989;54:1385–7.
[158] Rost TA, Lin H, Rabson TA, Baumann RC, Callahan DL. Deposition and analysis of lithium niobate and other lithium niobium oxides by rf magnetron sputtering. J Appl Phys 1992;72:4336–43.
[159] Tan S, Schlesinger TE, Migliuolo M. The role of Si_3N_4 layers in determining the texture of sputter deposited $LiNbO_3$ thin films. Appl Phys Lett 1996;68:2651–3.
[160] Fork DK, Anderson GB. Epitaxial MgO on GaAs(111) as a buffer layer for z-cut epitaxial lithium niobate. Appl Phys Lett 1993;63:1029–31.
[161] Lee SH, Song TK, Noh TW, Lee JH. Low-temperature growth of epitaxial $LiNbO_3$ films on sapphire (0001) substrates using pulsed laser deposition. Appl Phys Lett 1995;67:43–5.
[162] Levy M, Osgood RM, Liu R. Fabrication of single-crystal lithium niobate films by crystal ion slicing. Appl Phys Lett 1998;73:2293–5.
[163] Rabiei P, Günter P. Optical and electro-optical properties of submicrometer lithium niobate slab waveguides prepared by crystal ion slicing and wafer bonding. Appl Phys Lett 2004;85:4603–5.
[164] Rabiei P, Steier WH. Lithium niobate ridge waveguides and modulators fabricated using smart guide. Appl Phys Lett 2005;86:161115.
[165] Guarino A, Poberaj G, Rezzonico D, Degl'Innocenti R, Günter P. Electro-optically tunable microring resonators in lithium niobate. Nat Photonics 2007;1:407–10.
[166] Noguchi K, Mitomi O, Miyazawa H, Seki S. A broadband Ti:$LiNbO_3$ optical modulator with a ridge structure. IEEE J Lightwave Technol 1995;13:1164–8.
[167] Hu H, Milenin AP, Wehrspohn RB, Herrmann H, Sohler W. Plasma etching of proton-exchanged lithium niobate. J Vac Sci Technol A 2006;24:1012–5.
[168] Ting TL, Chen LY, Wang WS. A novel wet-etching method using joint proton source in $LiNbO_3$. IEEE Photon Technol Lett 2006;18:568–70.
[169] Gill DM, Jacobson D, White CS, Shi Y, Minford WJ, Harris A. Ridged $LiNbO_3$ modulators fabricated by a novel oxygen-ion implant/wet-etch technique. IEEE J Lightwave Technol 2004;22:887–94.
[170] Barry IE, Ross GW, Smith PGR, Eason RW. Ridge waveguides in lithium niobate fabricated by differential etching following spatially selective domain inversion. Appl Phys Lett 1999;74:1487–8.
[171] Hu H, Ricken R, Sohler W, Wehrspohn RB. Lithium niobate ridge waveguides fabricated by wet etching. IEEE Photon Technol Lett 2007;19:417–9.
[172] Lee YS, Kim GD, Kim WJ, Lee SS, Lee WG, Steier WH. Hybrid Si-$LiNbO_3$ microring electro-optically tunable resonators for active photonic devices. Optics Lett 2011;36:1119–21.
[173] Chen L, Xu Q, Wood MG, Reano RM. Hybrid silicon and lithium niobate electro-optical ring modulator. Optica 2014;1:112–8.
[174] Gebbie HA, Harding WR, Hilsum C, Pryce AW, Roberts V. Atmospheric transmission in the 1 to 14 μm region. Proc R Soc London A 1951;206:87–107.
[175] Sorokina IT, Vodopyanov KL, eds. Solid-state mid-infrared laser sources. Berlin-Heidelbrg, Germany, Springer-Verlag, 2003.
[176] Krier A, ed. Mid-infrared semiconductor optoelectronics. Berlin-Heidelberg, Springer-Verlag, 2006.
[177] Ebrahim-Zadeh M, Sorokina IT, eds., Mid-infrared coherent sources and applications. Berlin-Heidelberg, Germany, Springer-Verlag, 2008.
[178] Petrich W. Mid-infrared and Raman spectroscopy for medical diagnostics. Appl Spectrosc Rev 2001;36:181–237.
[179] Jean B, Bende T. Mid-IR applications in medicine. In: Sorokina, I.T., Vodopyanov, K.L., eds., Solid-state mid-infrared laser sources, Berlin-Heidelberg, Springer-Verlag, 2003.
[180] Ilev IK, Waynant RW, Mid-infrared biomedical applications. In: Krier, A., ed., Mid-infrared semiconductor optoelectronics, Berlin-Heidelberg, Springer-Verlag, 2006.
[181] Laser Components, Inc. (Accessed September 15, 2014 at http://www.lasercomponents.com.).

[182] AdTech Optics, Inc. (Accessed September 15, 2014 at http://www.atoptics.com.).
[183] Thorlabs Inc. (Accessed September 15, 2014 at http://www.thorlabs.com.).
[184] Judson Technologies, Inc. (Accessed September 15, 2014 at http://www.judsontechnologies.com.).
[185] Jalali B, Raghunathan V, Shori R, Fathpour S, Dimitropoulos D, Stafsudd O. Prospects for silicon mid-IR Raman lasers. IEEE J Sel Topics Quantum Electron 2006;12:1618–27.
[186] Soref R. Mid-infrared photonics in silicon and germanium. Nat Photonics 2010;4:495–7.
[187] Raghunathan V, Borlaug D, Rice R, Jalali B. Demonstration of a mid-infrared silicon Raman amplifier. Opt Express 2007;15:14355–62.
[188] Borlaug D, Fathpour S, Jalali S. Extreme value statistics in silicon photonics. IEEE Photonics J 2009;1:33–9.
[189] Raghunathan V, Shori R, Stafsudd OM, Jalali B. Nonlinear absorption in silicon and the prospects of mid-infrared silicon Raman laser. Phys Status Solidi A 2006;203:R38–40.
[190] Ma J, Fathpour S. Pump-to-stokes relative intensity noise transfer and analytical modeling of mid-infrared silicon Raman lasers. Opt Express 2012;20:17962–72.
[191] Soref RA, Emelett SJ, Buchwald WR. Silicon waveguided components for the long-wave infrared region. J Optics A 2006;8:840–8.
[192] Baehr-Jones T, Spott A, Ilic R, Spott A, Penkov B, Asher W, Hochberg M. Silicon-on-sapphire integrated waveguides for the mid-infrared. Opt Express 2010;18:12127–35.
[193] Mashanovich GZ, Milošević MM, Nedeljkovic M, Owens N, Xiong B, Teo EJ, Hu Y. Low loss silicon waveguides for the mid-infrared. Opt Express 2011;19:7112–9.
[194] Wong CY, Cheng Z, Chen X, Xu K, Fung CKY, Chen YM, Tsang HK. Characterization of mid-infrared silicon-on-sapphire microring resonators with thermal tuning. IEEE Photonic J 2012;4:1095–102.
[195] Shankar R, Bulu I, Lončar M. Integrated high-quality factor silicon-on-sapphire ring resonators for the mid-infrared. Appl Phys Lett 2013;102:051108.
[196] Imthurn G. The history of silicon-on-sapphire. White paper for Peregrine Semiconductor Corporation, 2007. (Accessed September 15, 2014 at http://www.psemi.com/articles/History_SOS_73-0020-02.pdf.).
[197] Chang YC, Paeder V, Hvozdara L, Hartmann J-M, Herzig HP. Low-loss germanium strip waveguides on silicon for the mid-infrared. Opt Lett 2012;37:2883–5.
[198] Malik A, Dwivedi S, Van Landschoot L, Muneeb M, Shimura Y, Lepage G, Van Campenhout J, Vanherle W, Van Opstal T, Loo R, Roelkens G. Ge-on-Si and Ge-on-SOI thermo-optic phase shifters for the mid-infrared. Opt Express 2014;22:28479–88.
[199] Khan S, Chiles J, Ma J, Fathpour S. Silicon-on-nitride waveguides for mid- and near-infrared integrated photonics. Appl Phys Lett 2013;102:121104.
[200] Chiles J, Khan S, Ma J, Fathpour S. High-contrast, all-silicon waveguiding platform for ultra-broadband mid-infrared photonics. Appl Phys Lett 2013;103:151106.
[201] Chiles J, Fathpour S. Silicon on lithium niobate: a hybrid electro-optical platform for near- and mid-infrared photonics. Proc. Conference on Lasers and Electro-Optics (IEEE/OSA CLEO 2014), Paper STh1M.6, San Jose, CA, June 2014.
[202] Chiles J, Fathpour S. Mid-infrared integrated waveguide modulators based on silicon-on-lithium-niobate photonics. Optica 2014;1:350–5.
[203] Sánchez S, Gui C, Elwenspoek M. Spontaneous direct bonding of thick silicon nitride. J Micromech Microeng 1997;7:111–3.
[204] Gui C, Elwenspoek M, Gardeniers JGE, Lambeck PV. Present and future role of chemical mechanical polishing in wafer bonding. J Electrochem Soc 1998;145:2198–204.
[205] Yamada A, Kawasaki T, Kawashima M. SOI by wafer bonding with spin-on glass as adhesive. Electron Lett 1987;23:39–40.
[206] Yamada A, Kawasaki T, Kawashima M. Bonding silicon wafer to silicon nitride with spin-on glass as adhesive. Electron Lett 1987;23:314–5.
[207] Cheng Z, Chen X, Wong CY, Xu K, Tsang HK. Mid-infrared suspended membrane waveguide and ring resonator on silicon-on-insulator. IEEE Photon J 2012;4:1510–9.
[208] Spencer H. Progress: its law and cause. In: Essays: scientific, political, and speculative, vol. I, New York, NY, D. Appleton and Company, 1891.